CHAPTER 3

Freezing and thawing of foods – computation methods and thermal properties correlation

H. Schwartzberg[1], R.P. Singh[2] & A. Sarkar[2]
[1]*Department of Food Science, University of Massachusetts, USA.*
[2]*Department of Biological and Agricultural Engineering, University of California – Davis, USA.*

Abstract

Correlations are derived for local water activities, a_w, unfrozen water contents, n_w, ice contents, n_I, effective heat capacities, C, thermal conductivities, k, and specific enthalpies, H, as functions of temperature, T, in foods at subfreezing conditions. The validity of the correlations has been demonstrated for many foods. The correlations can be used to provide thermal properties data for freezing and thawing calculations, including numerical solution of partial differential equations (PDEs) describing heat transfer during freezing and thawing. Finite element and finite difference methods for solving such PDEs are described, particularly enthalpy step methods. Local T versus time, t, histories for food freezing and thawing obtained by the use of these methods are presented.

1 Engineering calculations

Food process engineers often have to calculate heat transfer loads for freezing and thawing, how fast such heat can be transferred, how changing product or process variables affects transfer rapidity, how freezing rates and T differ in different parts of a product, and how T rises in frozen food exposed to abusive conditions. Thermal property correlations and computational methods presented here can be used for such calculations.

2 Freezing points

Pure water and normal ice, i.e. ice Ih, are in equilibrium at temperature T_o (273.16K, 0°C, or 32°F) at atmospheric pressure. This chapter deals with freezing

WIT Transactions on State of the Art in Science and Engineering, Vol 13, © 2007 WIT Press
www.witpress.com, ISSN 1755-8336 (on-line)
doi:10.2495/978-1-85312-932-2/03

and thawing of normal ice in foods. Other ice crystal forms exist at higher pressures [1].

2.1 Freezing point depression

Dissolved solutes depress water's freezing point. The greater the solute concentration, the greater the depression. As water in a solution changes to ice, solute concentrations increase in the remaining solution, and the equilibrium temperature, T, decreases. Equilibrium T for aqueous solutions during freezing and thawing are governed by eqn (1) [2]

$$\ln(a_w) = \ln(\gamma_w X_w) = -\frac{18.02\Delta H_{av}(T_o - T)}{RT_oT} \tag{1}$$

where a_w is water's thermodynamic activity, γ_w its activity coefficient, X_w its mole fraction in the solution, 18.02 its molecular weight, and ΔH_{av} its average latent heat of fusion between T_o and T. T_o and T are in degrees kelvin. The ideal gas law constant $R = 8.314$ kJ/(kg mol K). $\Delta H_{av} = \Delta H_o + 0.5(C_I - C_w)(T_o - T)$, where the heat capacity of ice $C_I = 2.093$ kJ/(kgK); C_w, the heat capacity of pure water averages 4.187 kJ/(kgK); and water's latent heat at T_o, $\Delta H_o = 333.57$ kJ/kg (143.4 BTU/lb).

$$\Delta H_{av}/TT_o \approx \Delta H_o/T_o^2$$

Therefore, with very little error,

$$\ln(a_w) = -\frac{18.02\Delta H_o(T_o - T)}{RT_o^2} \tag{2}$$

Equation (2) and methods based in part on earlier derivations [3–6] are used to derive thermal property correlations presented here. All the right-hand terms in eqn (2) except $(T_o - T)$ are constants. Thus, during freezing, $-\ln(a_w)$ is proportional to and is solely a function of $(T_o - T)$. Substituting for ΔH_o, R, and T_o, one obtains

$$\ln(a_w) = 0.00969T_C \tag{3}$$

where T_C is T in degree centigrade. Equation (3) provides a_w with less than 1% error at T_C as low as $-40°C$. Values of γ_w are difficult to predict for foods for $X_w < 0.8$, but for $X_w > 0.9$, $\gamma_w \approx 1.0$, and X_w can replace a_w in eqn (2), yielding Raoult's law for freezing,

$$\ln(X_w) = -\frac{18.02\Delta H_o(T_o - T)}{RT_o^2} \tag{4}$$

2.2 Bound water

Aqueous solutions contain both solvent water and water bound to solute molecules. Bound water acts like part of the solute, does not freeze, and does not contribute

to a_w or freezing point depression [7–10]. Thus X_{we}, the effective mole fraction of the solvent water in the solution, is

$$X_{we} = \frac{(n_w - bn_s)/18.02}{(n_w - bn_s)/18.02 + n_s/M_s} = \frac{n_w - bn_s}{(n_w - bn_s) + En_s} \tag{5}$$

where n_w is the total weight fraction of water in the solution, n_s the weight fraction of solute, b the mass of water bound per unit mass of solute, M_s is the solute's effective molecular weight, and $E = 18.02/M_s$. The effective molecular weight of a solute that dissociates is its molecular weight divided by the number of ions produced per solute molecule. Substituting X_{we} given by eqn (5) for a_w in eqn (2)

$$\ln(X_{we}) = \ln\left[\frac{n_w - bn_s}{n_w - bn_s + En_s}\right] = -\frac{18.02\Delta H_o(T_o - T)}{RT_o^2} \tag{6}$$

Foods usually contain many solutes. If none precipitates, their relative weight proportions do not change during freezing. Therefore, when constants E and b are determined by best fit methods, eqn (6) can be used for solute mixtures.

Equation (6) can also be used for moist solid foods with b representing both water bound to solutes and water adsorbed by insoluble solids per unit mass of solutes and insoluble solids combined. Riedel [7, 11–15] and Duckworth [8] list b for various foods. Pham [9] lists both bn_s and T_i, the food's initial freezing point.

$2(X_{we} - 1)/(X_{we} + 1)$ is the first term of a series expansion for $\ln(X_{we})$ [16]. For $X_{we} > 0.8$, it agrees with $\ln(X_{we})$ with less than 0.6% error. Substituting $2(X_{we} - 1)/(X_{we} + 1)$ for $\ln(X_{we})$ in eqn (6), one obtains

$$\frac{En_s}{n_w - (b - 0.5E)n_s} = \frac{En_s}{n_w - Bn_s} = \frac{18.02\Delta H_o(T_o - T)}{RT_o^2} \tag{7}$$

$B = b - 0.5E$. Errors caused by assuming $\ln(X_{we}) = 2(X_{we} - 1)/(X_{we} + 1)$ and $\Delta H_{av}/TT_o \approx \Delta H_o/T_o^2$ both increase as $(T_o - T)$ increases, but largely cancel one another. Therefore, if $\gamma_w = 1.0$ or if b also accounts for water nonideality, eqn (7) applies with less than 0.5% error even at −40°C. Applying eqn (7) at $T = T_i$, where $n_w = n_{wo}$, the weight fraction of water prior to freezing, one obtains

$$\frac{En_s}{n_{wo} - Bn_s} = \frac{18.02\Delta H_o(T_o - T_i)}{RT_o^2} \tag{8}$$

3 Water and ice weight fractions

Dividing eqn (8) by eqn (7), one obtains

$$\frac{n_w - Bn_s}{n_{wo} - Bn_s} = \frac{T_o - T_i}{T_o - T} \tag{9}$$

n_I, the weight fraction of ice in a food, $= n_{wo} - n_w$. Therefore,

$$n_I = (n_{wo} - Bn_s)\left[\frac{T_i - T}{T_o - T}\right] \tag{10}$$

Equations (9) and (10) can be used with both T and T_i in kelvin, degrees centigrade, and degrees fahrenheit. $n_s = (1 - n_{wo})$. If, for example, $T_i = -1°C$, half the freezable water will be frozen when $T = -2°C$, two-thirds when $T = -3°C$ and three-quarters when $T = -4°C$, and so on.

Bartlett [17, 18] was probably the first to use Raoult's law for freezing to predict n_I and the thermal properties of food, but his equations are complex. Equations (6), (7), or (10) or similar equations using b instead of B or with B omitted have been used to determine n_w and n_I [3, 19–24]. Fikiin [25] reviewed methods for predicting n_I from Eastern European literature.

4 Effective heat capacities

At $T > T_i$, i.e. in the unfrozen state, the heat capacity $C = C_o$. C_o is often assumed constant for freezing or thawing calculations. At $T < T_i$, i.e. for frozen or partly frozen foods, H the specific enthalpy a food can be obtained by summing the enthalpy contributions of the components

$$H = n_w \bar{H}_w + n_I H_I + n_s \bar{H}_s \tag{11}$$

where H_I is the specific enthalpy of ice, $\bar{H}_w$ the partial enthalpy of liquid water, and $\bar{H}_s$ the partial enthalpy of solids and solutes combined. X_w remains larger than 0.9 during most of the freezing process. Therefore, we can assume that $\bar{H}_w = H_w$, the specific enthalpy of pure water.

Food freezing takes place over a range of temperatures where the food's effective heat capacity $C = dH/dT$.

$$C = \frac{dH}{dT} = n_w \frac{dH_w}{dT} + H_w \frac{dn_w}{dT} + n_I \frac{dH_I}{dT} + H_I \frac{dn_I}{dT} + n_s \frac{d\bar{H}_s}{dT} \tag{12}$$

where dH_w/dT, dH_I/dT, and $d\bar{H}_s/dT$, respectively, equal C_w, the heat capacity of water; C_I, the heat capacity of ice; and C_s, the partial heat capacity of the nonaqueous components. Further, $-dn_I = dn_w$, $n_I = n_{wo} - n_w$, and $H_w - H_I = \Delta H_T$, ice's latent heat of fusion at T. Based on eqn (9)

$$\frac{dn_w}{dT} = \frac{(n_{wo} - Bn_s)(T_o - T_i)}{(T_o - T)^2} \tag{13}$$

Substituting for dn_w/dT from eqn (13), for $(n_w - Bn_s)$ from eqn (9) and noting that $\Delta H_o = \Delta H_T + (C_w - C_I)(T_o - T)$, one obtains after algebraic manipulation

$$C = C_F + \frac{(n_{wo} - Bn_s)(T_o - T_i)\Delta H_o}{(T_o - T)^2}. \tag{14}$$

where $C_F = n_s C_s + (n_{wo} - Bn_s)C_I + Bn_s C_w$. Figure 1 is a plot of eqn (14) based on measured C versus T values for codfish muscle [11]. For meats [12, 26], the height of the C peak at T_i decreases as fat content increases and water content decreases. Differential scanning calorimetry curves [27, 28] for sucrose, glucose, fructose,

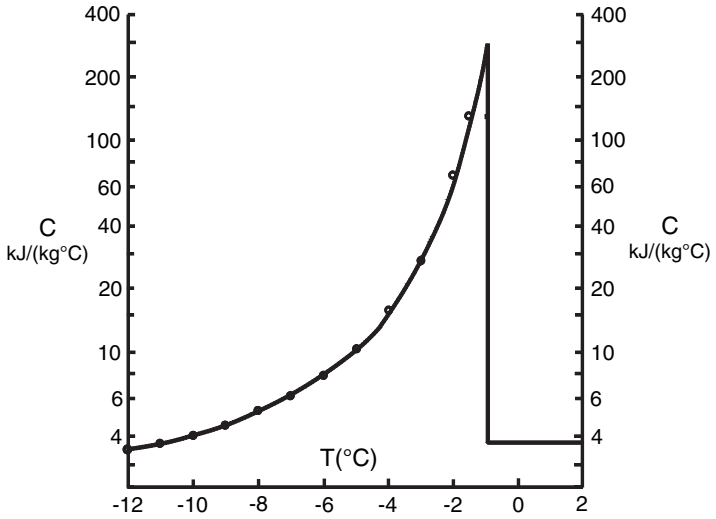

Figure 1: Effective heat capacity C versus T for cod above and below T_i, based on data of Riedel [11].

solutions of mixed sugars, orange juice, grape juice, raspberry juice, grapefruit juice, apple juice, cod, and tuna resemble Fig. 1 except for small irregularities around −40°C or shifts in C at low T.

Schwartzberg [3–5] and Chen [29–31] derived equations like eqn (14) but with b replacing B. Chen used M_s rather than $E = M_w/M_s$ as a variable. Succar and Hayakawa [32] used $(T_o - T)^n$ instead of $(T_o - T)^2$ in Schwartzberg's equation. The n values, empirically found for each food, were close to 2.0, e.g. 1.9.

5 Enthalpies

H values are measured with respect to a reference temperature, T_R, where H is assigned a value of zero. Riedel [11–15] and others used −40°C as T_R. If T_i is used as T_R, H will be negative at $T < T_i$ and positive at $T > T_i$.

Integrating eqn (14) between T_R and T, one obtains for $T < T_i$

$$H = (T - T_R)\left[C_F + \frac{(n_{wo} - Bn_s)\Delta H_o}{(T_o - T_R)}\left(\frac{T_o - T_i}{T_o - T}\right)\right] \tag{15}$$

For $T > T_i$, $H = C_o(T - T_i) + H(T_i)$, where $H(T_i)$ is the value of H at T_i. Thus,

$$H = (T_i - T_R)\left[C_F + \frac{(n_{wo} - Bn_s)\,\Delta H_o}{(T_o - T_R)}\right] + C_o(T - T_i) \tag{16}$$

5.1 Use of T_i as T_R

If $T_i = T_R$, eqn (15) yields for $T < T_i$

$$H_{T_i} = (T - T_i)\left[C_F + \frac{(n_{wo} - Bn_s)\Delta H_o}{(T_o - T)}\right] \tag{17}$$

H_{T_i} indicates that T_i is the reference temperature. For $T > T_i$

$$H_{T_i} = C_o(T - T_i) \tag{18}$$

H_{T_i} clearly $= 0$ when $T = T_i$.

5.2 Use of $-40°C$ as T_R

Using $-40°C$ as T_R in eqn (15) one obtains H_{-40}. For $T < T_i$

$$H_{-40}(T) = A + C_F T_C + \frac{(n_{wo} - Bn_S)\Delta H_o(T_i)}{T_C} \tag{19}$$

$A = 40C_F - [(n_{wo} - Bn_s)\Delta H_o T_i]/40$, and T_C and T_i are in degree centigrade. Figure 2 is a plot of experimental and predicted H versus T for lean beef [12] with T_i as T_R (right axis) or $-40°C$ as T_R (left axis). Best fit values of $(n_{wo} - Bn_s)\Delta H_o$ treated as a single variable, and of T_i, C_o, C_F were used in eqns (17)–(19). H versus T curves for other foods [3, 11–15, 26, 27, 30, 33–36] are similar. H changes more between $-40°C$ and T_i when n_{wo} is high and fat content is low. Pham *et al.* [35] and

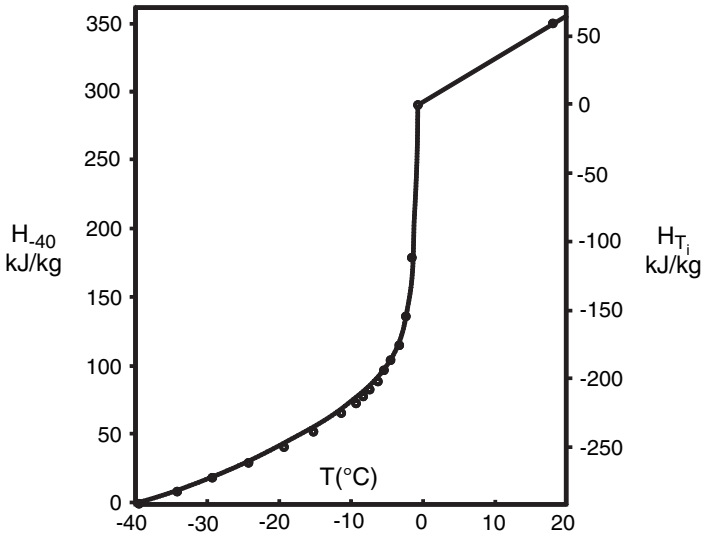

Figure 2: Enthalpy H versus T for lean beef: $T_R = -40°C$ left axis; $T_R = T_i$ right axis. Based on data of Riedel [12].

Lindsey and Lovatt [36] determined T_i and measured H_{-40} versus T for 43 foods and correlated their data by an equation formally identical to eqn (19). Correlation coefficients for their predicted and experimental H_{-40} were 0.999–1.000 for most foods and 0.992–0.998 for a few foods, mostly fatty ones. This degree of correlation lends support to the validity and utility of eqns (17)–(19).

6 Departures from equilibrium

Slow nucleation can cause T to drop below T_i before ice crystals form at chilled food surfaces and in chilled water drops suspended in nonaqueous media. Heterogeneous nucleation usually occurs around $T_i - 6°C$ for most foods, and subcooling is brief and confined to a shallow region near the foods surface. At high sucrose concentrations, e.g. 40% sucrose, nucleation may occur only at $T_i - 8°C$ and after several minutes at some chilled surfaces, e.g. aluminum, but occurs at $T_i - 6°C$ with much less delay at other chilled surfaces, e.g. stainless steel [37]. Slow nucleation or absence of ice nuclei can cause subcooling in isolated, small regions in food, but at normal freezing conditions is rarely detected by temperature measurement in normal size portions of foods with normal solute concentrations. Slow ice nucleation in dispersed drops of water in butter does cause appreciable subcooling when butter is frozen [38].

Based on comparisons between measured and predicted weights of frozen layers scraped off the inside wall of externally chilled, thin-wall, stainless-steel tubes, delayed nucleation affected short-term, frozen-layer growth rates at 20% sucrose concentration when the chilling medium temperature was less than 12°C below T_i but not when it was more than 12°C below T_i [37]. At high rates of heat removal and sucrose concentrations above 20%, experimentally measured frozen layer weights and thicknesses fell significantly below weights and thicknesses predicted by methods described later in this chapter. At 30% and 40% sucrose concentration or when 0.01% and 0.05% gelatin was added to 20% sucrose, the measured frozen layer weights and thicknesses were markedly lower than predicted weights and thicknesses [37]. Thus when heat removal rates are high and initial solute concentrations are much higher than normal or when agents that increase mass-transfer resistance are present, water mass transfer as well as heat transfer has to be taken into account in predicting freezing rates and T decrease rates. In such cases, freezing rates and T decrease rates predicted based on heat transfer analysis alone will be excessively high.

Water concentrations drop and solute concentrations rise outside ice crystal growth surfaces as water changes to ice at those surfaces. Water diffuses to the surfaces, but not fast enough to prevent surface concentrations from rising somewhat above the average solute concentration. Thus, T drops somewhat below its equilibrium value at the average concentration. When initial solute concentrations for foods are normal, i.e. T_i is around -1 to $-1.5°C$, subequilibrium T during freezing triggers increased nucleation and ice crystal branching, which prevents T from departing too far from equilibrium as long as T is greater than $-20°C$. But as T falls below $-30°C$, solution viscosity increases so markedly and therefore hinders water

diffusion to ice surfaces so that T can drop well below its equilibrium value. During commercial freezing, subequilibrium T can occur near outer surfaces of foods when the ambient temperature, T_a, is very low or h, the surface heat transfer coefficient, is very large, but only small parts of the food are affected. About 95% of freezable water will have frozen when T in the affected region reaches $-20°C$. Therefore, little ice formation is prevented; the use of the thermal properties equations derived here probably will not cause significant error for most freezing computations.

When cellular foods freeze, intercellular water nucleates and freezes more readily than water within cells. Water diffuses out of cells and freezes in intercellular space, particularly when freezing is slow [39–41]. This adversely affects texture after thawing. When freezing is rapid, ice nucleates and grows within cells and less water outdiffuses. Departures from concentration equilibrium occur over cell-sized distances at commercial freezing rates, but are small. Excess subcooling would cause ice nucleation and growth within cells. Predicted and measured T versus time histories for freezing of cellular foods agree reasonably well. Therefore, water out-migration from cells probably does not affect greatly the validity of the thermal properties equations presented here.

7 Volume changes

The specific volume of ice is 8.5% larger than that of water. Therefore, aqueous solutions expand as they freeze. Open gas-filled pores in fruits and vegetables can more than accommodate volume increases caused by freezing. Therefore, fruits and vegetable pieces may not expand during freezing. In liquid foods, freezing-induced expansion causes small amounts of freeze-concentrated liquid to move ahead of the freezing interface. Thermal properties for that freeze-concentrated liquid are difficult to predict. Expansions of fat-rich foods during freezing are also difficult to predict accurately.

8 Food composition variation

Compositions of foods vary naturally and can be changed artificially. If concentration remains uniform when water is added or removed from a food, the composition balance of the nonaqueous components affecting freezing will not change. Therefore, E and B will not change and can be used with the new n_{wo} and n_s in eqn (8) to find the new value of $(T_o - T_i)$. Then E, B, and the new n_{wo}, n_s and $(T_o - T_i)$ can be used as parameters in equations correlating n_w, n_I, C, and H versus T behavior, e.g. $C_F = n_s C_s + (n_{wo} - Bn_s)C_I + Bn_s C_w$ using the new n_s and n_{wo}.

During cooling, fats undergo heat-generating phase transitions both above and below T_i. This may cause problems in determining C and H for fat-containing foods. H versus T data for fat-rich foods containing at least moderate amounts of water, e.g. ice cream, sausage meat, cheeses, fat-containing meat, beef fat, pork fat, chicken fat, and butter, obey eqns (17) and (19); data for low water content lamb fat, beef suet and rendered beef fat do not [35, 36]. When eqns (17) and (19) are

valid, increasing fat content reduces ($n_{wo} - Bn_s$) and therefore reduces how much H changes during freezing.

9 Thermal conductivity

At $T > T_i$, the thermal conductivity in a food $k = k_o$, its value in the thawed state. k for ice is roughly 3.7 times as large as the k of water. Therefore, k increases markedly during freezing. In foods with oriented grainy structures, k is anisotropic and is greater parallel to the grain than across the grain. Ice crystals tend to grow with their axes parallel to the direction of heat removal. Therefore, k for frozen or partly frozen food may be anisotropic even in foods that initially did not have oriented structures.

Equation (20) predicts k fairly well at $T < T_i$. It is based on the assumption that increases in k are linearly proportional to the fraction of freezable water converted to ice [4, 5]. That assumption is reasonable when ice crystals grow parallel to the direction of heat removal.

$$k = k_f + (k_o - k_f)\left[\frac{n_w - Bn_s}{n_{wo} - Bn_s}\right] = k_f + (k_o - k_f)\left[\frac{T_o - T_i}{T_o - T}\right] \tag{20}$$

where k_o and k_f, respectively, are the thermal conductivities of the food in the unfrozen and in the fully frozen state. The thermal conductivity of ice increases as T decreases. Equation (21) partially accounts for that increase.

$$k = k'_f + m(T_i - T) + (k_o - k'_f)\left[\frac{T_o - T_i}{T_o - T}\right] \tag{21}$$

where m accounts for the increase in ice's thermal conductivity. k'_f is used instead of k_f. Agreement is good between experimental k and k predicted by eqn (21) when best fit m and k'_f are used. Figure 3 is a plot of eqns (20) and (21) and corresponding experimental k versus T data for beef [42]. k versus T plots for other foods [3, 34, 42–47] are similar. Willix *et al*. [44] presented T_i, gross composition, and measured k versus T data for 27 foods. They used an equation proposed by Pham and Willix [45] to correlate their k versus T data. Equation (21) correlates that data equally well and eqn (20) slightly less well.

Cogné *et al*. [34] and Reynaud *et al*. [47] provide methods that predict how food composition affects k versus T behavior at $T < T_i$, but which do not account for k anisotropy. Cogné *et al*. [34] obtained k versus T curves similar to those for eqns (20) and (21). They also found that effects of air inclusions on k in foamed foods could be predicted using the Maxwell–Euken equation, i.e.

$$k_d(T) = \frac{k(T)[2k(T) + k_a - 2\varepsilon(k(T) - k_a)]}{2k(T) + k_a + \varepsilon[k(T) - k_a]} \tag{22}$$

where $k_d(T)$ is the thermal conductivity of the foamed food (e.g. ice cream) at T, $k(T)$ the thermal conductivity of the foam-free food at T, k_a the thermal conductivity of air, and ε is the volume fraction of the food occupied by air. $k(T)$ for use in eqn (22) can be obtained by use of eqns (20) or (21).

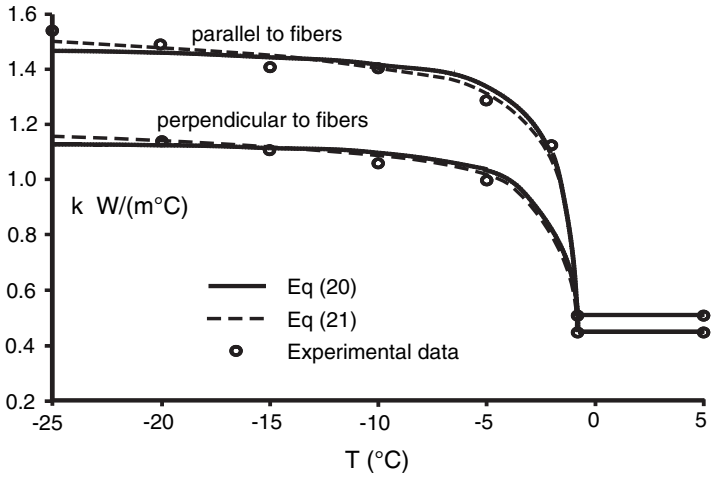

Figure 3: Thermal conductivity, k, perpendicular to and parallel to beef grain versus T for lean beef. Data of Jason and Long [43].

10 Freezing time estimation

Freezing times, t_f, are estimated to predict needed residence times for foods in freezers. As foods freeze, a frozen layer forms next to the outer surface and moves progressively inward. Ice grows and heat is removed mainly at or near the inward moving freezing interface. This heat transfers over progressively larger distances as freezing progresses, and the rate of inward front movement slows down. Plank's equation [48, 49] is based on freezing front movement in foods, where: (1) T initially $= T_i$ and is uniform; (2) complete freezing occurs at the boundary between the frozen and unfrozen zones; (3) $k = k_f$ in the frozen zone and k_o in the unfrozen zone, i.e. k changes sharply at T_i; (4) volume changes are negligible; and (5) freezing is complete when the front of the frozen layer reaches the food's center. Lopez-Leiva and Hallstrom [50] note that for the following shapes – infinite slab, infinite cylinder, infinite square rod, cylinder whose length equals its diameter, sphere and cube – Plank's equation and a similar equation, Rjutov's equations [51], reduce to

$$t_f = \frac{V_F \rho(\Delta H_E)[1 + 0.25Bi]}{hA_S(T_i - T_a)} \tag{23}$$

The food volume is V_F, its density is ρ, and its exposed surface area is A_S. The temperature of the cooling medium is T_a, and the coefficient of heat transfer between the food and the medium is h. ΔH_E is the amount of heat required to freeze a unit mass of the food. The Biot number $Bi = 2ha/k = Bi_f = 2ha/k_f$, where $2a$ is the thickness or diameter of the piece and k_f is the thermal conductivity of the frozen layer. *Note*: Some authors, e.g. Carslaw and Jaeger [52], use $Bi = ha/k$.

Based on the amount of water in a food, ΔH_E should equal $\Delta H_o(n_{wo} - Bn_s)$. Rjutov [51] used $\Delta H_E = [H(T_i) - H(-10°C)]$. $H(T_i)$ is the specific enthalpy of

the unfrozen food at T_i and $H(-10°C)$ the specific enthalpy at $-10°C$. If $T_i = -1°C$, Rjutov's $\Delta H_E = 9C_F + 0.9\Delta H_o(n_{wo} - Bn_s)$. Lopez-Leiva and Hallstrom [50] indicate that eqn (23) can be used to estimate t_f for shapes other than those previously cited by using the shortest dimension of the bulkiest section of the food as $2a$ and by multiplying Bi_f by 0.29 instead of 0.25. Many other methods [50, 53–56] have been proposed for adapting eqn (23) to deal with shapes other than those previously listed.

10.1 Thawing-time estimation

In thawing, an unfrozen layer moves progressively inward from the food's outer surfaces toward its center. Equation (23) can be used to predict thawing times by replacing k_f in Bi with k_o, the thermal conductivity of the food when thawed. Since k_f is several times as large as k_o, thawing is slower than freezing, particularly when h and a are large.

10.2 Precooling and subcooling

Engineers often have to predict the time, t_C, required to cool a food from an initial temperature, $T_1 > T_i$, to T_{2c}, a specified final T at the food's center, with T_{2c} usually being well below T_i. Many methods [45, 51–59] have been proposed for accomplishing that goal. Lopez-Leiva and Hallstrom [50] found Levy's method [57], eqn (24), to be simple and fairly accurate.

$$t_C = \frac{t_f(H_1 - H_2)[1 + 0.008(T_1 - T_i)]}{(n_{wo} - Bn_s)\Delta H_o} \tag{24}$$

where H_1 is the specific enthalpy at T_1, H_2 the specific enthalpy at T_2, the desired final T and t_f is obtained from eqn (23). When $T_R = T_i$, $H_1 = C_o(T_1 - T_i)$, and H_2 is obtained by substituting T_2 in eqn (17).

Pham's method [60], presented below, is one of the most accurate.

$$t_C = \frac{V\rho}{hA}\sum_{i=1}^{3}\frac{\Delta H_i}{\Delta T_i}\left[1 + \frac{(Bi)_i}{f_i}\right] \tag{25}$$

Here

$$f_1 = 6, \quad f_2 = 4, \quad f_3 = 6,$$

$$\Delta H_1 = C_o[T_1 - T_{fa}], \quad \Delta H_2 = \Delta H_o(n_{wo} - Bn_s), \quad \Delta H_3 = C_F[T_{fa} - T_{2a}],$$

$$(Bi)_1 = 2ha/k_o, \quad (Bi)_2 = [(Bi)_1 + (Bi)_3]/2, \quad (Bi)_3 = 2ha/k_f,$$

$$\Delta T_1 = [T_1 - T_{fa}]/\ln[(T_1 - T_a)/(T_{fa} - T_a)], \quad \Delta T_2 = [T_{fa} - T_a], \quad \text{and}$$

$$\Delta T_3 = [T_{fa} - T_{2a}]/\ln[(T_{fa} - T_a)/(T_{2a} - T_a)].$$

The mean effective freezing temperature in degree centigrade $T_{fa} = T_i - 1.5$. $T_{2a} = T_{2c} - (Bi)_3(T_{2c} - T_a)/[2(Bi)_3 + 2]$, where T_{2a} is the average final temperature and T_{2c}, the desired final center temperature.

11 Heat transfer coefficients

Uncertain values for h limit the accuracy of freezing and thawing calculations. Correlations for h are only moderately accurate and usually apply only for flow channels unimpeded by shelf supports, product surfaces not resting on support grids, and for fully developed flow. Local values of h vary markedly on meat carcass surfaces [61] and to moderate extents on other food surfaces. Local h can be determined accurately by analyzing recorded T versus time behavior for a highly conductive dummy load insulated at its nonexposed surfaces and placed at different sites in a freezer. The load should be shaped like the product or like part of it, depending on whether an overall h or h values for different sites on a product are desired.

12 Unsteady-state freezing and thawing

T versus time, t, and position behaviors during unsteady-state freezing and thawing are described by well-known partial differential equations (PDEs) and associated initial conditions (ICs) and boundary conditions (BCs) [52, 62]. A PDE for symmetric heat transfer in infinite slabs, infinite cylinders and spheres is

$$C\rho\frac{\partial T}{\partial t} = \rho\frac{\partial H}{\partial t} = \frac{1}{r^{\nu-1}}\frac{\partial}{\partial r}\left[r^{\nu-1}k\frac{\partial T}{\partial r}\right] \tag{26}$$

For slabs, $\nu = 1$ and r is the distance from the center plane. For cylinders, $\nu = 2$ and r is the distance from the cylinder axis. For spheres, $\nu = 3$ and r is the distance from the spheres center. For three-dimensional (3D)objects [52, 62],

$$C\rho\frac{\partial T}{\partial t} = \rho\frac{\partial H}{\partial t} = \frac{\partial}{\partial x}\left[k\frac{\partial T}{\partial x}\right] + \frac{\partial}{\partial y}\left[k\frac{\partial T}{\partial y}\right] + \frac{\partial}{\partial z}\left[k\frac{\partial T}{\partial z}\right] \tag{27}$$

where x, y, and z are distances along Cartesian coordinates. When heat transfer is symmetric, it is convenient to use the object's center as the origin for the coordinates. The IC usually used is $T = T_1$ for all r or all x, y, and z at $t = 0$, but heat transfer PDEs can be solved analytically or numerically if the internal values of T initially are nonuniform. T_1 can be greater, equal to, or less than T_i. For freezing and thawing, the convective BC is used most frequently, i.e.

$$k\left[\frac{\partial T}{\partial r}\right]_j = h_j[(T_a)_j - T_j] \tag{28}$$

The subscript j means at the jth surface; h_j, T_j and $(T_a)_j$, respectively, are the heat transfer coefficient, object temperature, and the external medium temperature at that surface. Often equal h_j are assumed; actual h_j usually differ. $(T_a)_j$ also differ, but usually less markedly than h_j does. If $h_j = \infty$, $T_j = (T_a)_j$. If $h_j = 0$, $(\partial T/\partial r)_j = 0$. $(\partial T/\partial r) = 0$ is also used as a BC at center points or center planes in objects where heat transfer is symmetric.

Cooling due to evaporation of water from exposed surfaces occurs when unwrapped food is frozen. Heating due to water condensation on food surfaces occurs during thawing. Such cooling and heating significantly affect freezing and

thawing rates and local T versus t behavior, but can be accounted for by modifying eqn (28) to account for water vapor transfer to or from exposed surfaces and associated heat release or heat absorption at those surfaces.

13 Explicit numerical solution of PDE

Equation (26) can be solved approximately but fairly accurately by machine computation using explicit methods, e.g. Euler's forward difference method.

To treat one-dimensional (1D), symmetric heat transfer, an object is divided into n lamina, the outermost and center lamina being $0.5\Delta r$ thick and all others Δr thick. $\Delta r = a/(n-1)$, a being the object's half thickness or radius. Values of T are defined or sought at aligned points, one at the object's center, one at its outer surface, and all others at the centers of all other lamina, all points being Δr apart. The T at the points are identified by subscript j indicating how many Δr increments separate the point from the object's center, and by superscript i indicating the current time step.

Geometric factors relate lamina volumes to $(\Delta r)^{\nu}$ and lamina surface areas to $(\Delta r)^{\nu-1}$. The net rate of heat flow across a lamina's surfaces equals the lamina volume times $C_j^i \rho(\partial T_j/\partial t)$. After common terms and $(\Delta r)^{\nu-1}$ cancel from this equation, the geometric factors for lamina volume and surface area, respectively, become α and β, which vary with position.

For interior points

$$T_j^{i+1} = T_j^i + \left[\frac{\Delta t}{\alpha_j C_j^i \rho(\Delta r^2)}\right] \times [(\beta_{j+1/2})k_{j+1/2}^i(T_{j+1}^i - T_j^i) - (\beta_{j-1/2})k_{j-1/2}^i(T_j^i - T_{j-1}^i)] \tag{29}$$

$k_{j+1/2}^i$ is obtained by averaging k at T_{j+1}^i and T_j^i and $k_{j-1/2}^i$ by averaging k at T_{j-1}^i and T_j^i. For $T < T_\mathrm{i}$, k is obtained by substituting T in eqn (20) or eqn (21). For $T > T_\mathrm{i}$, $k = k_\mathrm{o}$. For $T < T_\mathrm{i}$, C_j^i is obtained by substituting T_j^i for T in eqn (14). If $T > T_\mathrm{i}$, $C_j^i = C_\mathrm{o}$. ρ is assumed constant.

At $j = 0$, the center of the object,

$$T_0^{i+1} = T_0^i + \frac{2\nu\Delta t[k_{1/2}^i(T_1^i - T_0^i)]}{(\Delta r)^2 C_0^i \rho} \tag{30}$$

$\nu = 1$ for infinite slabs, 2 for infinite cylinders, and 3 for spheres

At $j = n$, the surface of the object,

$$T_n^{i+1} = T_n^i + \left[\frac{\Delta t}{\alpha_n C_n^i (\Delta r)^2}\right] \times [h\beta_n(\Delta r)(T_\mathrm{a} - T_n^i) - \beta_{n-1/2}k_{n-1/2}^i(T_n^i - T_{n-1}^i)] \tag{31}$$

Equations (29)–(31) are solved numerically by machine computation to obtain T_j^{i+1} for $j = 0$ to n. The T_j^{i+1} then becomes the T_j^i used in the next time step.

Table 1: Values of geometric factors for different shapes [63].

	Shape		
	Infinite slab	Infinite cylinder	Sphere
α_j	1	j	$j^2 + 1/12$
$\beta_{j+1/2}$	1	$j + 1/2$	$(j + 1/2)^2$
$\beta_{j-1/2}$	1	$j - 1/2$	$(j - 1/2)^2$
α_n	1/2	$(n - 1/4)/2$	$(n^2 - n/2 + 1/12)/2$
β_n	1	n	n^2

α_j, $\beta_{j+1/2}$, $\beta_{j-1/2}$, α_n, and β_n for infinite slabs, infinite cylinders, and spheres are listed in Table 1.

Computation becomes unstable if Δt is too large. Stability is provided by use of the smallest Δt obtained from eqns (32)–(34) treated as equalities.

$$\Delta t \leq \frac{\alpha_j C_j^i \rho (\Delta r)^2}{\beta_{j+1/2} k_{j+1/2}^i + \beta_{j-1/2} k_{j-1/2}^i} \tag{32}$$

$$\Delta t \leq \frac{C_o^i \rho (\Delta r)^2}{2\nu k_{1/2}^i} \tag{33}$$

$$\Delta t \leq \frac{\alpha_n C_n^i \rho (\Delta r)^2}{h\beta_n (\Delta r) + \beta_{n-1/2} k_{n-1/2}^i} \tag{34}$$

Equations (32)–(34) are those effectively used by Mannaperuma and Singh [63] for the enthalpy step method (discussed later). The allowable Δt varies as freezing or thawing proceeds, and should be re-evaluated after each time step.

When eqns (29)–(31) were solved for typical freezing conditions by machine computation, 700–2,000 time steps were used for infinite slabs, 370–1,000 steps for infinite cylinders, and 130–1,500 steps for spheres. The number of steps needed is not only inversely proportional to a^2 and proportional to $n^2(n + 1)$, but also depends on $Bi_f = 2ha/k_f$, T_1, T_a, and T_{2c}.

14 Implicit numerical solution of PDE

Larger Δt can be used without instability by using implicit methods, e.g. the Crank–Nicholson method [62, 64, 65]. When using the Crank–Nicholson method, $(T^i + T^{i+1})/2$ replaces each T^i on the right-hand side of eqns (29)–(31). For symmetric heat transfer in infinite slabs, infinite cylinders, and spheres, the Crank–Nicholson equation corresponding to eqn (29) is

$$\frac{2C_j^i \rho \alpha_j (\Delta r)^2}{\Delta t}(T_j^{i+1} - T_j^i) = [\beta_{j+1/2} k_{j+1/2}^i (T_{j+1}^i - T_j^i + T_{j+1}^{i+1} - T_j^{i+1})] + [\beta_{j-1/2} k_{j-1/2}^i (T_{j-1}^i - T_j^i + T_{j-1}^{i+1} - T_j^{i+1})] \tag{35}$$

Equations (30) and (31) can be converted to Crank–Nicholson form in similar fashion. Because two or three unknowns appear in each of the n equations used to calculate new T, one has to solve these equations simultaneously. Fortunately, the equations are linear and the coefficients for unknown terms lie on or next to the principal diagonal of the coefficient matrix, i.e. the matrix is tridiagonal. Such equations can be solved readily using a simple, Gauss elimination based subroutine, TRIDAG [66].

15 Lee's method

In Lee's method [65, 67], each T^i on the right-hand side of eqns (29)–(31) is replaced by $(T^i + T^{i+1} + T^{i-1})/3$ and the time step doubled, so that on the left-hand side of eqns (29)–(31) $(T^{i+1} - T^{i-1})/(2\Delta t)$ replaces $(T^{i+1} - T^i)/(\Delta t)$.

Again, two or three unknowns appear in each equation, simultaneous solution of n equations having a tridiagonal coefficient matrix is required, and TRIDAG can be used in solving those equations. Lee's method has the advantage of using C and k for the middle of a time step rather than the C and k at the start of the steps. T^{i-1} is not available for the first time step. Therefore, the Crank-Nicholson method should be used for the first time step.

One can use much larger Δt with both Lee's and Crank–Nicholson's methods than for the explicit method, but if Δt is too large, 'jumping' and T oscillations occur as T passes through T_i. Lee's method and the Crank–Nicholson method save computing time, but for 1D symmetric freezing and thawing the absolute amount of time saved is small.

16 Enthalpy step method

By replacing $C(\Delta T)$ with ΔH, eqns (29)–(31) can be rewritten so as to compute changes in enthalpy, H, during Δt [63, 68, 69]. Use of H based on $T_\mathrm{R} = T_\mathrm{i}$ is convenient when solving these equations:

$$H_j^{i+1} = H_j^i + \left[\frac{\Delta t}{\alpha_j \rho \left(\Delta r^2\right)}\right] \times [(\beta_{j+1/2})k_{j+1/2}^i(T_{j+1}^i - T_j^i) - (\beta_{j-1/2})k_{j-1/2}^i(T_j^i - T_{j-1}^i)] \tag{36}$$

$$H_0^{i+1} = H_0^i + \frac{2\nu\Delta t[k_{1/2}^i(T_1^i - T_0^i)]}{(\Delta r)^2\rho} \tag{37}$$

and

$$H_n^{i+1} = H_n^i + \left[\frac{\Delta t}{\alpha_n \rho(\Delta r)^2}\right] \times [h\beta_n(\Delta r)(T_\mathrm{a} - T_n^i) - \beta_{n-1/2}k_{n-1/2}^i(T_n^i - T_{n-1}^i)] \tag{38}$$

Once the H_j^{i+1} are obtained, the corresponding T_j^{i+1} in degree centigrade are found from eqns (17) or (18) rearranged. If $H_j^{i+1} > 0$

$$T_j^{i+1} = T_\mathrm{i} + \frac{H_j^{i+1}}{C_\mathrm{o}} \tag{39}$$

and if $H_j^{i+1} < 0$

$$T_j^{i+1} = \frac{F - \sqrt{F^2 - 4C_\mathrm{F}LT_\mathrm{i}}}{2C_\mathrm{F}}. \tag{40}$$

where $L = (n_\mathrm{wo} - Bn_\mathrm{s})\Delta H_\mathrm{o}$ and $F = (H_j^{i+1} + L + C_\mathrm{F}T_\mathrm{i})$.

To prevent computational instability, the Δt used must satisfy all of eqns (32)–(34). The enthalpy step method described is essentially that of Mannaperuma and Singh [63], who used equations in terms of volumetric enthalpies, $H_V = H\rho$, and in terms of volumetric heat capacities, $C_V = C\rho$, when calculating Δt.

Use of the enthalpy step method prevents T from jumping over T_i and eliminates errors caused by use of C at the start of a time step rather than at its middle. Use of k that apply at the start of time steps still causes some error.

16.1 Sample results for the enthalpy step method

In the enthalpy step based computations discussed below,

$$T_1 = 10°\mathrm{C}, \quad T_\mathrm{a} = -40°\mathrm{C}, \quad T_\mathrm{i} = -1°\mathrm{C}, \quad T_{2\mathrm{c}} = -18°\mathrm{C}$$

$(n_\mathrm{wo} - Bn_\mathrm{s})\Delta H_\mathrm{o} = 260$ kJ/kg, $C_\mathrm{o} = 3.5$ (kJ/kg °C), $C_\mathrm{F} = 2.05$ (kJ/kg °C), $\rho = 1050$ kg/m^3, $k_\mathrm{o} = 0.0005$ kW/(m °C), $k_\mathrm{f} = 0.0015$ kW/(m °C), and k for $T < T_\mathrm{i}$ were calculated using eqn (20).

Freezing and thawing times and T versus r and t histories were computed for infinite slabs, infinite cylinders and spheres for $a = 0.005$, 0.01, and 0.02 m and $h = 30$, 60, 120, 600, and 1,200 W/(m^2 °C). Calculated freezing times, t_f, for combinations of these h and a are given in Table 2. In industrial freezers, h is almost always less than 600 W/(m^2 °C). The $h = 600$ and 1,200 W/(m^2 °C) values are used to show how $Bi_\mathrm{f} = 2ha/k_\mathrm{f}$ affects freezing times.

The data listed in Table 2 and corresponding T versus r and t data were calculated using programs written in Quick Basic implemented on an IBM computer with a Windows 98 operating system. Computing times ranged from 1.3 to 2.8 s for infinite slabs, 0.5–2.5 s for infinite cylinders, and 0.3–2.9 s for spheres, and were greater at low h and Bi_f, and, in most cases, greater for small a.

At low Bi_f, t_f was roughly inversely proportional to h and roughly proportional to a. At larger Bi_f, h had less influence on t_f; and t_f was slightly less than proportional to a^2, with t_f approaching proportionality to a^2 at very large Bi_f.

Calculated thawing times (not listed in Table 2) were only moderately longer than corresponding calculated t_f at low Bi, where overall heat transfer rates depend mainly on h. At larger Bi, k influences overall heat transfer rates more, and calculated thawing times were much larger than corresponding t_f.

Table 2: Freezing times for infinite slabs, infinite cylinders, and spheres for different h and a combinations.

a (m)	h (W/m^2 °C)	Bi_f	Infinite slab t_f (s)	Infinite cylinder t_f (s)	Spheres t_f (s)
0.005	30	0.2	1,617	805	532
0.005	60	0.4	849	421	278
0.005	120	0.8	464	229	151
0.005	600	4	157	79	53
0.005	1,200	8	118	60	41
0.01	30	0.4	3,394	1,684	1,111
0.01	60	0.8	1,855	917	603
0.01	120	1.6	1,086	538	359
0.01	600	8	474	240	164
0.01	1,200	16	398	203	139
0.02	30	0.8	7,421	3,670	2,413
0.02	1,200	32	1,438	737	503

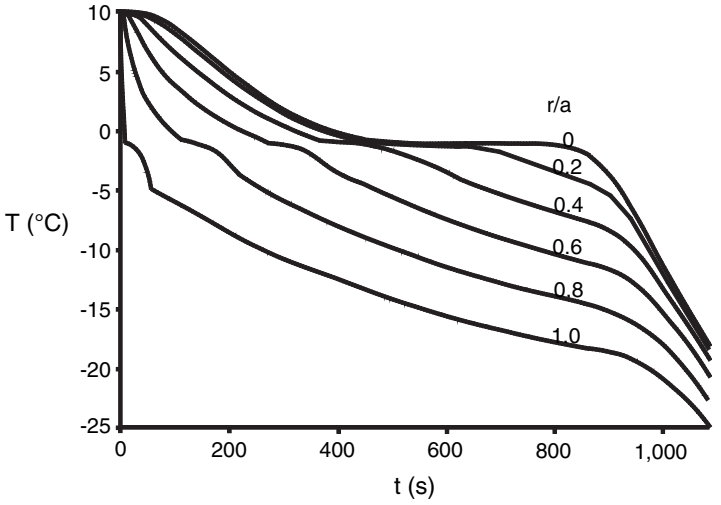

Figure 4: Predicted temperature, T, versus time, t, behavior at $0.2r/a$ intervals during freezing of a 0.02-m thick infinite slab when $T_a = -40$°C, $h = 120$ W/m^2 °C, and the previously listed thermal properties apply.

Figure 4 depicts computed T versus t at different r/a during the freezing of an infinite slab where $a = 0.01$ m and $h = 120$ W/(m^2 °C). Figure 5 shows computed T plotted versus r/a at different t for the same situation. For infinite slabs and all a or h, T varied roughly linearly with r/a over most of the frozen zone during freezing front penetration. During freezing front penetration, T in outer parts of the

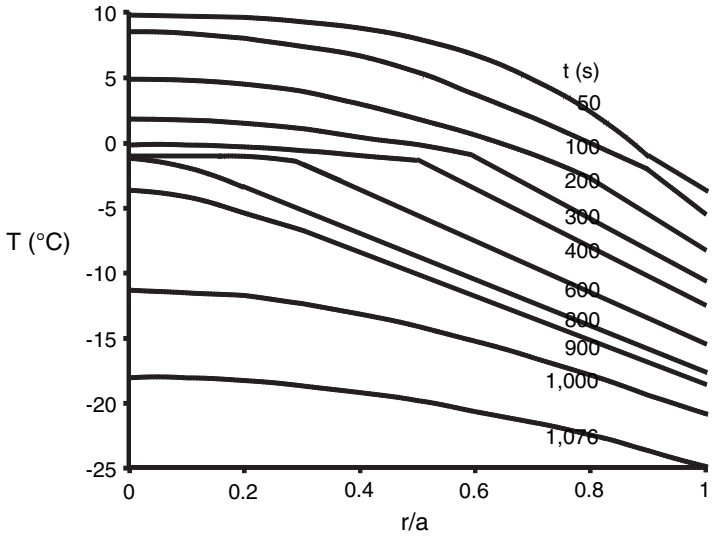

Figure 5: Predicted temperature, T, versus r/a behavior at selected times, t, during freezing of a 0.02-m thick infinite slab when $h = 120\,\mathrm{W/m^2}\ ^\circ\mathrm{C}$, $T_a = -40^\circ\mathrm{C}$, and the previously listed thermal properties apply.

frozen zone varies roughly linearly with $\ln(a/r)$ for infinite cylinders, and roughly linearly with (a/r) for spheres.

Mannaperuma and Singh [63] compared experimental freezing and thawing time data from the literature with results computed using the enthalpy step method and obtained agreement similar to that obtained by Lee's method. Toumi *et al.* [70] obtained good agreement between experimental t_f and T versus t data for cylindrical string beans and corresponding results computed by the enthalpy step method.

17 Multidimensional problems

Program for multidimensional problems are more complex and require more computer time to run than 1D problems.

17.1 Enthalpy step method

Mannaperuma and Singh [69] developed enthalpy step methods for freezing and thawing problems involving finite cylindrical domains and two-dimensional (2D) and 3D rectangular domains.

A Cartesian grid for a rectangular block of food, X long, Y wide, and Z high would have points $\Delta x = X/2J$ apart in the x direction, $\Delta y = Y/2K$ apart in the y direction and $\Delta z = Z/2M$ apart in the z direction, where J, K, and M, respectively, are half the number of x, y, and z layers in the grid. T and H at these points are

labeled $T^i_{j,k,m}$ and $H^i_{j,k,m}$ with i indicating at the current t. Again $(i+1)$ indicates at $t+\Delta t$. The subscripts j, k, and m, respectively, indicate the number of Δx, Δy, and Δz steps between a point and the x, y, z origin. Subscript j runs from $-J$ to J. At the x midplane of the grid $j=0$. Similarly, k and m, respectively, run from $-K$ to K and $-M$ to M; with $k=0$ and $m=0$, respectively, indicating the y and z midplanes of the grid.

At interior points in the grid,

$$H^{i+1}_{j,k,m} = H^i_{j,k.m} + \left(\frac{\Delta t}{\rho}\right) \times [P^i_j - P^i_{j-1} + P^i_k - P^i_{k-1} + P^i_m - P^i_{m-1}] \quad (41)$$

where

$$P^i_j = \frac{k^i_{j+1/2,k,m}(T^i_{j+1,k,m} - T^i_{j,k,m})}{(\Delta x)^2} \quad (42)$$

$$P^i_k = \frac{k^i_{j,k+1/2,m}(T^i_{j,k+1,m} - T^i_{j,k,m})}{(\Delta y)^2} \quad (43)$$

and

$$P^i_m = \frac{k^i_{j,k,m+1/2}(T^i_{j,k,m+1} - T^i_{j,k,m})}{(\Delta z)^2} \quad (44)$$

where P^i_{j-1}, P^i_{k-1} and P^i_{m-1}, respectively, are obtained by replacing subscript j by $(j-1)$ in eqn (42), subscript k by $(k-1)$ in eqn (43) and subscript m by $(m-1)$ in eqn (44). For 2D problems, eqn (44) and subscript m are not used, and P^i_m and P^i_{m-1} are dropped from eqn (41).

For symmetric heat transfer: (1) a grid for only one eighth of a 3D object or for only one quarter of a 2D object need be used; (2) $T^i_{-1,k,m} = T^i_{1,k,m}$ for T adjacent to the $j=0$ plane; and (3) similar conditions apply for T adjacent to the $k=0$ and $m=0$ planes and at the grid's center. Thus H and T for points along these planes and at the grid's center can be determined by use of eqns (41)–(44) without need of special equations for those points.

For convective heat transfer at the $j=J$ surface

$$H^{i+1}_{J,k,m} = H^i_{J,k,m} + \frac{\Delta t}{\rho} \times \left[\frac{2h_J(T^i_{aJ} - T^i_{J,k,m})}{\Delta x} - 2P^i_{J-1} + (P^i_k - P^i_{k-1} + P^i_m - P^i_{m-1})_J\right] \quad (45)$$

where h_J and T_{aJ} are the heat transfer coefficient and external medium temperature at $j=J$. Subscript J after $(P^i_k - P^i_{k-1} + P^i_m - P^i_{m-1})$ means that these P are evaluated along $j=J$. Similar equations apply for the surfaces at $j=-J$, $k=K$ or $-K$, and $m=M$ or $-M$. Cases where h and/or T differ at different object surfaces and heat transfer and temperature profiles consequently are not symmetric can be

handled readily. Equation (45) with subscript m dropped and with P^i_m and P^i_{m-1} left out can be used to compute H^i_J, along the sides of 2D objects.

Equation (45) is not valid at the edges and corners of surfaces of 3D objects or at corners of 2D objects. At all points except the corners on the edge between the J and K surfaces

$$H^{i+1}_{J,K,m} = H^i_{J,K,m} + \frac{\Delta t}{\rho}[2Q^i_J - 2P^i_{J-1} + 2Q^i_K - 2P^i_{K-1} + (P^i_m - P^i_{m-1})_{J,K}] \tag{46}$$

where

$$Q^i_J = \frac{h_J[(T_a)_J - T^i_{J,K,m}]}{\Delta x} \tag{47}$$

$$Q^i_K = \frac{h_K[(T_\mathrm{a})_K - T^i_{J,K,m}]}{\Delta y} \tag{48}$$

Subscript J, K after $(P^i_m - P^i_{m-1})$ in eqn (46) indicates that m and $m-1$ lie on the edge between surfaces J and K. Equations similar to eqns (46)–(48) apply for edges between other combinations of surfaces. $H^{i+1}_{J,K}$ for corners in 2D objects can be computed from eqns (46) to (48) with subscript m dropped and P^i_m and P^i_{m-1} deleted.

At the corner formed by the intersection of the J, K, and M surfaces

$$H^{i+1}_{J,K,M} = H^i_{J,K,M} + \frac{2\Delta t}{\rho}[(Q^i_J)_{K,M} + (Q^i_K)_{J,M} + (Q^i_M)_{J,K} - (P^i_{J-1} + P^i_{K-1} + P^i_{M-1})] \tag{49}$$

where

$$(Q^i_J)_{K,M} = \frac{h_J[(T_\mathrm{a})_J - T^i_{J,K,M}]}{\Delta x} \tag{50}$$

$(Q^i_K)_{J,M}$ and $(Q^i_M)_{J,K}$ are similarly defined. H^{i+1} for the other corners are determined from equations similar to eqn (49) and with other Q combinations, e.g. $(Q^i_{-J})_{K,M}$, $(Q^i_K)_{-J,M}$, and $(Q^i_M)_{-J,K}$.

Mannaperuma and Singh [69] also provided equations for calculating H^{i+1} at surfaces where heat flux is prescribed or where T remains constant.

To prevent computational instability when treating 2D or 3D problems, Δt must be less than or equal to the smallest limiting Δt for grid interior points and points on outer surfaces, edges, and corners. Except at the very start of computation, the smallest Δt usually will be either that for an interior point or that for the coldest corner for freezing or for the hottest corner for thawing. We derived equations for limiting Δt for all sites in a grid, but present only those usually needed, i.e. those for Δt for interior points and for corners.

For grid interior points, usable Δt are given by

$$\Delta t \leq \frac{\rho C^i_{j,k,m}}{S^i_j + S^i_k + S^i_m} \tag{51}$$

where

$$S^i_j = \frac{k^i_{j+1/2,k,m} + k^i_{j-1/2,k,m}}{(\Delta x)^2} \tag{52}$$

$$S^i_k = \frac{k^i_{j,k+1/2,m} + k^i_{j,k-1/2,m}}{(\Delta y)^2} \tag{53}$$

and S^i_m is defined similarly.

For the corner between surfaces J, K, and M, the maximum usable Δt is

$$\Delta t = \frac{\rho C^i_{J,K,M}}{2[(N^i_J)_{K,M} + (N^i_K)_{J,M} + (N^i_M)_{J,K}]} \tag{54}$$

where

$$(N^i_J)_{K,M} = \frac{h_J(\Delta x) + k^i_{J-1/2,K,M}}{(\Delta x)^2} \tag{55}$$

$$(N^i_K)_{J,M} = \frac{h_K(\Delta y) + k^i_{J,K-1/2,M}}{(\Delta y)^2} \tag{56}$$

Subscript J means at $j = J$, K means at $k = K$, and K, M means along the edge between K and M. $(N^i_M)_{J,K}$ is provided by an equation similar to eqn (55) or (56).

Equation (54) is used for only the coldest corner for freezing or for only the hottest corner for thawing. Use of the smallest Δt given by eqn (51) or (54) prior to each time step provides stable computation. If h is very large, short-lived T oscillations occur near the start of computation at edge points close to the chosen corner, but do not affect predicted T significantly at later times. Such oscillation can be prevented by initially using smaller Δt, e.g. $\Delta t = 0.25$ times the smallest Δt obtained from eqns (51) and (54) for the first 40 time steps.

Pham [71] provides a way to use larger, fixed Δt without instability by combining elements from the enthalpy step method and Lee's method.

17.1.1 Computed results for 2D, enthalpy step method

A computer program written in Quick Basic was used to solve eqns (41)–(50) for symmetrical freezing in infinitely long, square slabs of food. The Δt used was the smaller of the two determined through use of eqn (51) at the square's center and eqn (54) at one of the square's corners. Computer runs for freezing were carried out using the same thermal properties, IC and BC used for the enthalpy computer runs for 1D freezing. Figure 6 shows computed isotherms for -0.75°C, -1°C, -5°C,

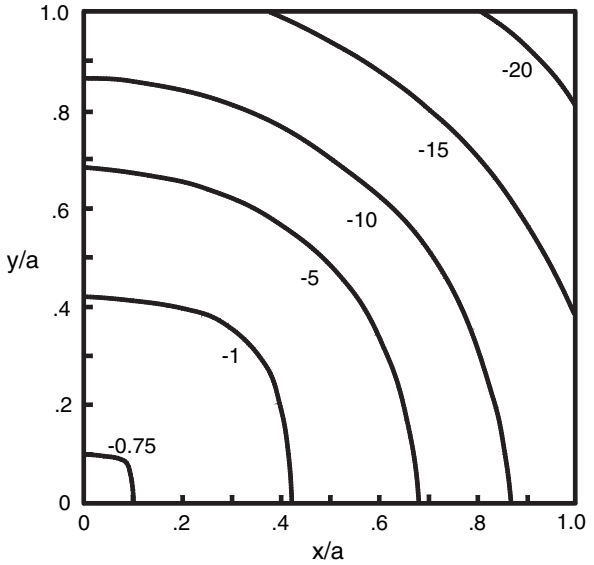

Figure 6: Predicted −0.75°C, −1°C, −5°C, −10°C, −15°C, and −20°C isotherms for one quarter of an infinitely long, 0.02-m wide square rod 322 s after the start of cooling when $h = 120$ W/m^2 °C and $T_a = -40$°C and the physical properties previously listed apply.

−10°C, −15°C, and −20°C at $t = 322$ s for one-quarter of a 0.02-m thick square rod for $h = 120$ W/(m^2 °C) and $T_a = -40$°C.

Similar computations were made for all h and a used for 1D calculations. As h and Bi_f decreased, distances between 5°C-spaced isotherms increased. For the 0.02-m thick square rod, t_f ranged from 1,720 s for $h = 30$ W/(m^2 °C) to 234 s for $h = 1{,}200$ W/(m^2 °C), and computation times ranged from 57 s at $h =$ 30 W/(m^2 °C) to 28 s at $h = 600$ W/(m^2 °C). Computation times for the other thicknesses were not greatly different.

17.2 Explicit, temperature step method

Equations (41), (45), (46) and (49) are converted into equations that directly provide T^{i+1} instead of H^{i+1} by using $C(\Delta T)$ instead of ΔH. The time steps needed to maintain stability are the same as for the enthalpy step method. Again, direct computation of T^{i+1} causes T to jump over the initial freezing point, T_i, and errors arise due to use of C at the start of time steps. Therefore, the enthalpy step method is preferred over the T-step method for multidimensional problems.

17.3 Alternating-direction implicit (ADI) methods

The Crank–Nicholson method and Lee's finite difference method usually generate too many simultaneous equations when used directly for multidimensional

problems. ADI methods reduce the number of equations that have to be solved simultaneously at one time and are preferred. In the Peaceman and Ratchford method [72], the Crank–Nicholson method is used in one direction and the explicit method in all other directions for one time step. The directions in which each method is used are changed for the next time step. The method has been used for problems in the x–y plane and for symmetric heat conduction in finite cylinders. It is stable for all Δt for two dimensions, but is only conditionally stable for three dimensions. Other ADI methods and how such methods are used for multidimensional, food-freezing problems are described in references listed by Cleland [65].

18 Irregular shape and nonuniform composition

Fairly complex programs based on finite difference methods have been used to treat freezing of irregularly shaped foods [73–78] and nonuniform composition [73, 76].

18.1 Coordinate transformation

Califano and Zaritzky [79] used coordinate transformations to generate irregular quadrilateral grids that fitted closely the shapes of irregular 2D objects. Predicted T versus t histories for points in those grids were computed by a finite difference method for freezing and thawing of minced beef and tylose. Good agreement with experimental data was obtained. Computation times were short, computer codes less complex and computer memory requirements much smaller than for a finite element method (FEM) based program providing similar accuracy.

18.2 Finite element method

Nowadays, programs for computing freezing and thawing behavior in irregularly shaped food and food of nonuniform composition are based mainly on the use of FEM.

18.2.1 Literature about FEM use for freezing and thawing problems

Journal articles [80–91] dealing with food freezing and thawing problems solved through the use of FEM rarely discuss FEM basics or provide program details. Information about noncommercial FEM programs can be found in M.S. and Ph.D.theses, e.g. [92]. Several books [93–95] provide good, lengthy treatments of FEM basics. Briefer treatment of FEM basics for the widely used Galerkin method and discussion of how FEM can be used for freezing and thawing problems are presented below. Books by Lewis *et al*. [96] and Huang and Usmani [97], and chapters in references [92, 94, 95] treat use of FEM for heat transfer problems.

18.2.2 Galerkin's method of weighted residuals

In the FEM, the space in an object is subdivided into adjoining, nonoverlapping elements sharing common boundaries and junction points (nodes). Accuracy is better when more elements are used, but computation time increases [93, 96].

FEMs are based on minimizing values of integrals over the entire object space and over elements in that space. Development of FEM by means of the method of weighted residuals [93–95] is examined below. FEM development by means of variational methods [98] will not be covered.

Though symmetric freezing in infinite slabs is treated efficiently by finite difference methods, FEM-based treatment of such freezing will be used in explaining the method of weighted residuals. Consider a slab of width $2a$ convectively cooled at a and $-a$. T varies spatially only in the x direction. Therefore linear elements can be used.

Though $C_V(\partial T/\partial t)$ is often used instead of $\partial H_V/\partial t$ in programs analyzing heat transfer by FEM, use of $\partial H_V/\partial t$ is advantageous when treating freezing or thawing. In rearranged form, the PDE for heat conduction in an infinite slab is

$$\frac{\partial}{\partial x}\left(k\frac{\partial T}{\partial x}\right) - \frac{\partial H_V}{\partial t} = 0 \tag{57}$$

Because of symmetry, only the region between $x = 0$ and $x = a$ is treated. The BCs are $\partial T/\partial x = 0$ at $x = 0$, and $k\partial T/\partial x = h(T - T_a)$ at $x = a$. The line from $x = 0$ to $x = a$ is divided into $(m - 1)$ linear elements, lying end to end, with m nodes, each node lying at a junction point between elements. Though element lengths could be unequal, equal lengths are used here. Let T and $(\partial H_V/\partial t)$ that approximately solve eqn (57) and satisfy the BC and IC be

$$T_A = \sum_{j=1}^{m} N_j(T_j) \quad \left(\frac{\partial H_V}{\partial t}\right)_A = \sum_{j=1}^{m} N_j\left(\frac{\partial H_V}{\partial t}\right)_j \tag{58}$$

The N_j are assumed functions of x, and T_j and $(\partial H_V/\partial t)_j$ are values at nodes j.

There very likely will be error or a residual, R, when assumed T_A and $(\partial H_V/\partial t)_A$ are substituted in eqn (57). The method of weighted residuals seeks to determine $(\partial H_V/\partial t)_j$ and T_j that cause R to be small over the entire problem domain, i.e. between $x = 0$ and $x = a$ in this case. It does this by choosing m linearly independent weighting functions, W_j, and requiring that

$$\int_0^a RW_j dx = 0. \tag{59}$$

If so, $R \approx 0$ for the entire slab. In the Galerkin method [93], the W_j are chosen to be the same as the N_j. This requires that

$$\int_0^a N_j\left[\frac{\partial}{dx}k\left(\frac{\partial T_A}{\partial x}\right) - \left(\frac{\partial H_V}{\partial t}\right)_A\right]dx = 0 \quad j = 1, 2, \ldots, m \tag{60}$$

Equation (57) applies at any point in the domain. Therefore, it applies for any collection of points defining an element in the domain. Thus, we can write

$$\int_{(e)} N_j^{(e)}\frac{\partial}{dx}\left(k\left(\frac{\partial T_A}{\partial x}\right)^{(e)}\right)\mathrm{d}x - \int_{(e)} N_j^{(e)}\left(\frac{\partial H_v}{\partial t}\right)_{\mathrm{A}}^{(e)}\mathrm{d}x = 0 \quad j = 1, 2, \ldots, r \tag{61}$$

The symbol (e) indicates that the range of integration is restricted to one element. In eqn (61), the integral for an element is written as the sum of two integrals, r is the number of nodes in an element, and $N_j^{(e)}$ serves as an interpolating function as well as a weighting function for the element. For line elements, $r = 2$; the N_j that ultimately provide suitable spatial continuity for T, $\partial T/\partial x$, and $\partial H_V/\partial t$ are

$$N_1 = \frac{x_2 - x}{x_2 - x_1} \qquad N_2 = \frac{x - x_1}{x_2 - x_1} \tag{62}$$

where the superscript (e) has been omitted.

$\partial T_A/\partial x = \Sigma T_j(dN_j/dx)$, which replaces $\partial T_A/\partial x$ in the first integral in eqn (61). Then, the first integral is integrated by parts. This reduces the x derivative order by one, satisfying derivative continuity requirements for FEM use [93] and yields

$$k\left(\frac{\partial T}{\partial x}\right)\bigg|_2 - k\left(\frac{\partial T}{\partial x}\right)\bigg|_1 + \int_1^2 k\left[\frac{\mathrm{d}N}{\mathrm{d}x}\right]\{T\}^{(e)}\frac{\mathrm{d}N_j}{\mathrm{d}x}\mathrm{d}x \tag{63}$$

$[\mathrm{d}N/\mathrm{d}x]$ is a row vector, $\{T\}^{(e)}$ is a column vector and $k(\partial T/\partial x)|_1$ and $k(\partial T/\partial x)|_2$ are $k(\partial T/\partial x)$ evaluated at node 1 and node 2, respectively. Expression (63) replaces the first integral in eqn (61). Then $\Sigma N_j(\partial H_V/\partial t)_j$ is substituted for $(\partial H_V/t)_A$ in the second integral, and it and the unintegrated part of the first integral are integrated. This yields a pair of equations. Similar pairs are obtained for each element.

Node 2 of a line element is also node 1 for the next element. Pairs of equations for $(\partial H_V/\partial t)_j$ at the same node are added to solve for the $(\partial H_V/t)_j$. Thus, at all interior nodes $-k(\partial T/\partial x)_1$ and $k(\partial T/\partial x)_2$ for neighboring element cancel. Since no element precedes $x = 0$, $-k(\partial T/\partial x)_1$ is not cancelled there. Since no element follows $x = a$, $k(\partial T/\partial x)_2$ is not cancelled there. From the BC, $(\partial T/\partial x) = 0$ at $x = 0$, and $k(\partial T/\partial x) = h(T_m - T_\mathrm{a})$ at $x = a$, i.e. at node m, where $T_j = T_m$. Integration by parts, whether in one dimension, two dimensions (Green's theorem), or three dimensions (Gauss's theorem) introduces BC into equations pertaining to nodes on external boundaries [93].

Complete integration of eqn (61) yields matrix eqn (64). Details of intermediate steps in that process are provided in references [93–95].

$$[C]\{H_V'\} + ([K_\mathrm{c}] + [K_\mathrm{h}])\{T\} = \{R_h\}. \tag{64}$$

In eqn (64), braces { } indicate a column vector, and brackets [ ] a square matrix, 2×2 in the present case. $(H_V')_j$ means $(\partial H_V/\partial t)_j$, and

$$\{T\} = \begin{Bmatrix} T_1 \\ T_2 \end{Bmatrix} \qquad \{H_V'\} = \begin{Bmatrix} (H_V')_1 \\ (H_V')_2 \end{Bmatrix} \tag{65}$$

In this example, T_1 and T_2 are current values.

$$[K_\mathrm{c}] = \frac{k_A}{(\Delta x)}\begin{bmatrix} 1 & -1 \\ -1 & 1 \end{bmatrix} \tag{66}$$

$(\Delta x) = (x_2 - x_1)$, the element length, and $k_A = (k_1 + k_2)/2$.

$[K_h]\{T\}$ and $\{R_h\}$ are utilized only at the node at $x = a$, where they are

$$[K_\mathrm{h}]\{T\} = hT_m \quad \{R_h\} = hT_\mathrm{a} \tag{67}$$

Matrix $[C]$ has two forms: (1) the 'consistent' form

$$[C] = \frac{\Delta x}{6}\begin{bmatrix} 2 & 1 \\ 1 & 2 \end{bmatrix} \tag{68}$$

and (2) the 'lumped' form

$$[C] = \frac{\Delta x}{2}\begin{bmatrix} 1 & 0 \\ 0 & 1 \end{bmatrix} \tag{69}$$

Lumped $[C]$ should be used when H_V changes are determined by explicit methods [93], as in the present case.

Because column vectors $\{T\}$ and $\{H'_V\}$ contain two rows, there are two equation for each element. $(2m - 1)$ equations are obtained after eqn (64) is evaluated for all elements. The T_j are known; the $(H'_V)_{j\_}$ have to be found. Except for the first and last elements, (H'_V) in the second equation for an element is the same as (H'_V) in the first equation for the following element. At internal nodes, the two equations for $H'_V)$ are added before solving for the $(H'_V)_j$. This yields m uncoupled algebraic equations, one for each node. In the present case, these equations are the same as those used to determine $(\partial H_V/\partial t)$ at points in infinite slabs by the explicit, enthalpy step, finite difference method. The FEM-based equations provide no advantage in the present case, but methods and concepts used in deriving them can be employed profitably in FEM treatment of more complex freezing and thawing problems.

18.2.3 Explicit time-stepping methods for FEM

Explicit FEMs generate uncoupled algebraic equations, even for complex 2D and 3D freezing and thawing problems. For such equations,

a. $(H_V)_j^{i+1} = (H_V)_j^i + (H'_V)_j(\Delta t)$ for all j;
b. $(T_j)^{i+1}$ are computed from the $(H_V)_j^{i+1}$ for all j by using eqn (40);
c. the $(T_j)^{i+1}$ then become the $(T_j)^i$ used to compute new k_j, $(H_V)_j^i$ and $(H'_V)_j$ for all j;

Steps (a)–(c) are repeated until a desired $(T_j)^{I+1}$ is reached at a given node.

Program sections for the time-stepping part of explicit FEM are easy to write, but small Δt must be used to prevent instability [91, 93, 98]. Step-by-step determination of allowable Δt is often burdensome for complex 2D or 3D freezing and thawing problems. Therefore, a trial Δt is often used and Δt is reduced when instability or oscillation is detected [91]. After Δt is reduced, the $(H'_V)_j^i$, $(H_V)_j^{i+1}$, and $(T)_j^{i+1}$ for the step just completed are recalculated. Pham [99] devised a self-correcting, enthalpy-based, explicit FEM which is stable even when large, normally intolerable Δt are used.

18.2.4 Implicit time-stepping methods for FEM

FEM programs often use implicit time-stepping methods, particularly methods that are stable for all Δt and which permit use of large Δt. These methods generate large sets of coupled equations that have to be solved simultaneously. In the backward difference method (BDM), the $(H'_V)_j^i$ are obtained by using T_j^{i+1} instead of T_j^i in $\{T\}$. This generates equations containing variables from both time i and time $i+1$. BDM are oscillation free, can use relatively large Δt, but when Δt was too large have yielded inaccurate results for FEM-based treatments of freezing and thawing problems [91].

The extended trapezoid rule (ETR), $H_j^{i+1} = H_j^i + (\Delta t)((H'_V)_j^i + (H'_V)_j^{i+1})/2$, has also been used in programs for solving freezing and thawing problems by FEM. It has also yielded inaccurate results when Δt was too large [91].

18.2.5 2D problems

Triangular elements can fit irregular curves closely and completely fill areas surrounded by such curves. Thus, they are used most frequently for 2D FEM problems [93], e.g. computing freezing and thawing behavior in infinitely long rods of any shape and in axisymmetric or nearly axisymmetric bodies such as hamburgers, straight sausages, finite cylinders, and many fruit. Figure 7 shows finite element layouts for half cross-sections of Rome apple and Bartlett pears [100]. The apple layout contains 39 triangular elements and 28 nodes; the pear has 37 triangular elements and 29 nodes.

Quadrilateral elements can be used for 2D problems involving domains well-fitted by such elements. Highly irregular curved areas have been treated by FEM using small numbers of 'isoparametric' elements with curved edges, and nodes at points along their edges as well as at vertices between edges [93, 94].

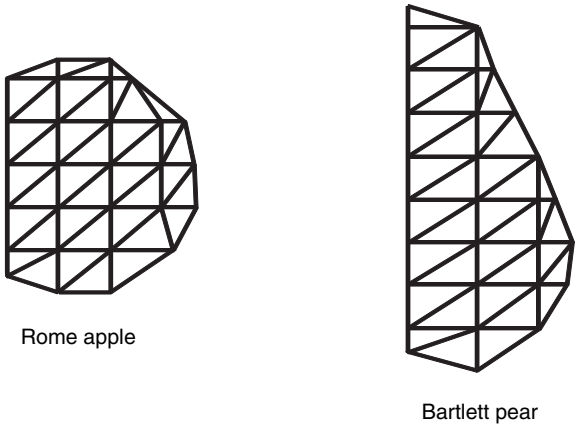

Figure 7: Layout of triangular elements for Rome apple and Bartlett pear treated as axisymmetric bodies by Carrol *et al.* [100].

Equation (63) is also used for triangular elements. $[C]$ and $[K_c]$ now contain A_e, the element area, as a prefactor and 3×3 matrices, e.g. $[C] = (A_e/3)[G]$, where $[G]$ is a matrix, 3×3 in the present case, whose only nonzero entries are 1, 1, 1 along its principal diagonal. $\{T\}$ and $\{H'_V\}$ now have three rows, and three equations per element are generated initially. Thus, 117 equations are generated for the apple layout. Adding equations for (H'_V) at the same node reduces this number to 28, one equation for each node.

Combining, arranging, and solving FEM equations can be complicated even for the simple element layout used for the apple. Solving such equations by matrix methods is facilitated by node-numbering practices and program subroutines that sequence equations so coefficients for the T_j form a compact group around the main diagonal of the coefficient matrix for the overall set of equations [93, 94, 97].

18.2.6 3D problems

Tetrahedral elements provide good volume-filling and surface-fitting ability and frequently are used for 3D objects. Figure 8, an element layout for a quarter of an ellipsoid whose axes are all of different length, contains 1,979 tetrahedral elements and 491 nodes [91]. Because of symmetry, only a quarter of the ellipsoid had to be modeled. Far fewer triangular elements could have been used if the ellipsoid had been axisymmetric. Axial and lateral symmetry should be exploited whenever possible when using FEM.

Small numbers of 3D isoparametric elements with curved surfaces have been used for FEM analysis of heat transfer in highly curved 3D domains [101].

Equation (64) is used for tetrahedral elements also, but with 4×4 matrices, four-row $\{T\}$ and $\{H'_V\}$, and four equations per element. Thus, 7,916 equations are generated for elements in the ellipsoid in Fig 8. Equations relating to the same $(H'_V)_j$ are added, yielding 491 equations for the $(H'_V)_j$ at nodes. Scheerlinck *et al*. [91] used a commercial enthalpy-based FEM program run on interconnected parallel

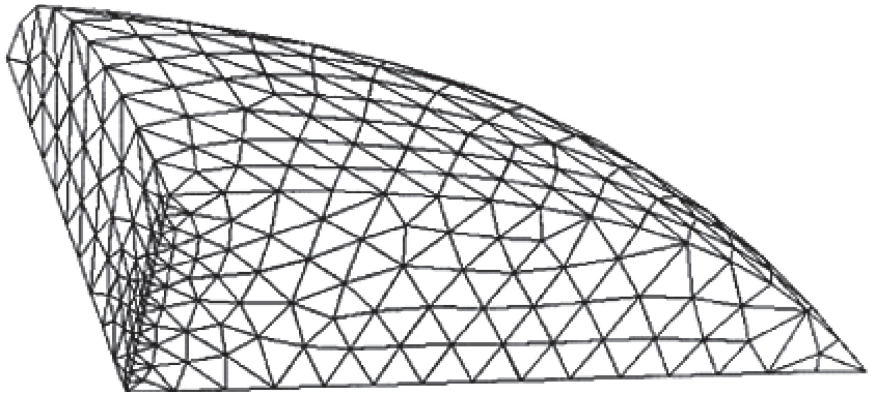

Figure 8: Layout of tetrahedral elements used in modeling freezing in an ellipsoid whose sides are of unequal length. Based on Scheerlinck *et al*. [91].

computers to predict T versus t behavior during freezing for points along the ellipsoid's smallest axis. They also treated the same problem by FEM-based programs and approaches of their own devising.

18.2.7 Meshing

Dividing object domains into elements is called meshing or discretizing. Large numbers of elements have been used for meshing irregular or even fairly regular 3D objects. Cheung *et al*. [102] describe a number of meshing methods. Meshing is often implemented by programs or subprograms that generate domain-filling arrays of contiguous elements, label all elements and nodes, determine the spatial coordinates of nodes, and store that information in computer files. These programs sometimes are used in conjunction with image acquisition equipment and software, computer-aided design (CAD) software, and/or food image libraries [103].

18.2.8 Steps in solving freezing 3D problems by FEM

Full FEM treatment of unsteady-state, 3D freezing problems by enthalpy methods involves: (1) generating a shape-fitting mesh with adequate numbers of elements; (2) keeping track of the elements, nodes, and nodal spatial coordinates; (3) using nodal coordinates to formulate weighting functions for the elements; (4) setting up equations for T and H'_V at the nodes in each element; (5) combining and ordering these equations to yield a smaller number of well-ordered equations for the H'_V at nodes; (6) entering h and T_a values for equations for surface nodes; (7) inserting initial or new T for the nodes; (8) using these T to compute k and H_V at the nodes; (9) solving equations to determine H'_V at all the nodes; (10) using the H'_V at nodes and a suitable Δt to determine H_V^{i+1} at nodes; (11) using eqn (40) to determine corresponding T^{i+1} values; and (12) repeating steps (7) to (11) for successive time steps until a set freezing time has elapsed or a desired final T is reached at some node. Step (6) is repeated whenever h or T_a changes at some or all surface nodes.

18.2.9 FEM Software

Commercial FEM software often provides graphical user interfaces, is user friendly [103, 104], can be used without understanding FEM principles, and has been used to treat complex [91] and noncomplex [87, 89, 90] freezing and thawing problems including problems involving freezing-induced mechanical stress [90]. Expensive, general purpose commercial FEM software, e.g. ABAQUS/Standard [105], ANSYS [106], run on powerful computers were used to solve some of these problems. Now such problems can often be handled on work stations or up-to-date PCs by less expensive FEM software, e.g. FEMLAB [107], ALGOR Professional Heat Transfer [108], ANSYS Professional/Introductory Level, and TOPAZ3D [109], many of which are available at still lower cost for academic use. Students can obtain even cheaper FEM software, e.g. ABAQUS Student Edition [110], for personal use. FEM programs for freezing and thawing have been and will continue to be written using general purpose, math-based software such as FORTRAN and MATLAB [91, 111] that run on PCs or work stations. CALFEM [112], an interactive program for teaching FEM, can be used as an FEM toolbox for MATLAB.

Nomenclature

A	half thickness or radius of piece of food (m)
a_w	water activity
A	$40C_F - [(n_{wo} - Bn_s)\Delta H_o T_i]/40$, see eqn (19)
A_e	area of triangular element
A_s	exposed surface area of piece of food
b	water binding factor (kg bound and adsorbed water)/(kg solute + solids)
B	$(b - 0.5E)$
Bi	Biot number $= 2ha/k$
Bi_f	Biot number in the fully frozen state $= 2ha/k_f$
C	effective heat capacity of food during freezing or thawing [kJ/(kgK)]
C_V	$C\rho$, volumetric heat capacity of food [kJ/(m^3 K)]
C_o	heat capacity of food in thawed state [kJ/(kg K)]
C_F	heat capacity of food in fully frozen state [kJ/(kg K)]
C_I	heat capacity of ice [2.09 kJ/(kg K)]
C_s	partial heat capacity of solute + solids [kJ/(kg K)]
C_w	heat capacity of water [4.18 kJ/(kg K)]
$[C]$	capacitance matrix in finite element treatment of freezing and thawing
E	$18.02/M_s$
f_i	numerical factor for ith period of freezing in eqn (25)
F	$(H_j^{i+1} + L + C_F T_i)$ (kJ/kg)
G	square matrix with ones along its principal diagonal and zeros elsewhere
h	surface heat transfer coefficient between cooling or thawing medium and piece of food [kW/(m^2 K)]
H	enthalpy per unit mass of food (kJ/kg)
H_I	specific enthalpy of ice (kJ/kg)
H_s	partial enthalpy of the solids and solutes combined (kJ/kg)
$H(T_i)$	value of H at T_i (kJ/kg)
H_{Ti}	enthalpy per unit mass of food using as T_i as T_R (kJ/kg)
H_{-40}	enthalpy per unit mass of food using as -40°C as T_R (kJ/kg)
H_V	$H\rho$, volumetric enthalpy of food (kJ/m^3)
H_w	specific enthalpy of liquid water (kJ/kg)
H_w	partial enthalpy of liquid water (kJ/kg)
H_1	enthalpy per unit mass of food at T_1 (kJ/kg)
H_2	enthalpy per unit mass of food at T_2 (kJ/kg)
H'_V	$\partial H_V/\partial t$ (kW/m^3)
ΔH_{av}	mean latent heat of fusion of water between 273.16 K and T (kJ/kg)
ΔH_E	amount of heat removed per unit mass during freezing (kJ/kg), in eqn (23)

ΔH_i	heat per unit mass removed in ith period of freezing (kJ/kg), in eqn (25)
ΔH_o	latent heat of fusion of water at 273.16 K (333.57 kJ/kg)
ΔH_T	latent heat of fusion of water at T (kJ/kg)
J	half the number of (Δx) layers in a heat transfer computation grid, at the grid's outer surface in the positive x direction
k	thermal conductivity of food [kW/(m K)]
k_a	thermal conductivity of air [kW/(m K)]
k_A	average thermal conductivity in finite element [kW/(m K)]
k_d	thermal conductivity of dispersion [kW/(mK)]
k_f	thermal conductivity of food in fully frozen state in eqn (20) [kW/(m K)]
k'_f	thermal conductivity of food in frozen state in eqn (21) [kW/(m K)]
k_o	thermal conductivity of unfrozen food in eqn (20) [kW/(m K)]
K	half the number of (Δy) layers in a heat transfer computation grid, at the grid's outer surface in the positive y direction
$[K_c]$	conductance matrix in FEM, see eqns (64) and (66)
$[K_h]$	convective matrix in FEM, see eqns (64) and (67)
L	$(n_{wo} - Bn_s)\Delta H_o$ (kJ/kg)
M_s	effective molecular weight of solutes and solids combined
M	half the number of (Δz) layers in a heat transfer computation grid, at the grid's outer surface in the positive z direction
m	thermal conductivity correction factor used in eqn (21) to account for increase in ice's thermal conductivity as T decreases below T_i
m	The number of nodes in a set of $(m-1)$ line elements eqn (60)
n	(number of temperature nodes -1) for finite difference calculations involving unidirectional freezing and thawing
n_I	weight fraction of ice in partially frozen food (kg ice/kg food)
n_s	weight fraction of solutes or solids in food (kg solids/kg food)
n_w	weight fraction of unfrozen water in partially frozen food $n_{wo} - n_I$
n_{wo}	overall weight fraction of water in food (kg water/kg food)
N_j	weighting and interpolation factor in FEM, see eqns (58), (60) and (61)
$(N_J^i)_{K,M}$	term defined by eqn (55)
$(N_K^i)_{J,M}$	term defined by eqn (56)
P_j^i	term defined by eqn (42)
P_k^i	term defined by eqn (43)
P_m^i	term defined by eqn (44)
Q_J^i	term defined by eqn (47)
Q_K^i	term defined by eqn (48)
r	distance from the center or center plane of an object (m) eqns (26)–(28)
r	number of nodes in an element, e.g. as in eqn (62)
Δr	$a/(n-1)$, distance between temperature nodes (m)

R	perfect gas law constant
R	residual in FEM integral, see eqn (59)
$\{R_h\}$	T_a-based convective column vector in FEM, see eqns (64) and (67)
S_j^i	term defined by eqn (52)
S_k^i	term defined by eqn (53)
T	food temperature, local food temperature (K) (°C sometimes)
T_1	initial T (K or °C)
T_2	final T (K or °C)
T_{2a}	average final T of food (K or °C) used in eqn (25)
T_{2c}	desired final T at center of food (K or °C)
T_a	temperature of cooling or heating medium (K or °C)
T_A	T function specified by eqn (58)
T_C	T in °C
T_{fa}	mean effective temperature during freezing stage 2 in eqn (25) (°C)
T_i	initial freezing point of solution or food (K or °C)
T_o	freezing point of pure water (273.16 K)
T_R	reference temperature for enthalpy of food (T_i or -40°C)
ΔT_i	temperature driving force during ith period in eqn (25)
t	time (s)
t_C	time to bring food from $T_1 > T_i$ to $T_2 < T_i$; eqns (24) and (25) (s)
t_f	freezing time for food initially at T_i (see eqn 23) (s)
V_F	volume of piece of food (m^3)
W_j	weighting factor in FEM based on method of weighted residuals, eqn (59)
X	extent of Cartesian grid in x direction (m)
X_w	mole fraction of water in solution or food, eqns (1) and (4)
X_{we}	effective mole fraction of water in solution or food, eqns (5) and (6)
x	lateral distance from the center or a side of object (m)
Δx	X/J, distance between sets of temperature nodes in the x direction (m)
Y	extent of Cartesian grid in y direction (m)
y	distance back from center of object or from its front surface (m)
Δy	X/K, distance between sets of temperature nodes in the y direction (m)
Z	extent of Cartesian grid in z direction (m)
z	vertical distance from center of object or from its bottom surface (m)
Δz	Z/M, distance between sets of temperature nodes in the z direction (m)
α	volume geometric factor for lamina
β	geometric factor for surface area of lamina
γ_w	activity coefficient of water
ν	geometric index: 1 for infinite slabs, 2 for infinite cylinders, 3 for spheres
ε	porosity (m^3 pores/m^3 food)
ρ	density of food (kg/m^3)

Subscripts

A	function designed to satisfy PDE, BC, and IC in FEM
i	ith term in summation in eqn (25)
j	at the jth surface of an object eqn (28)
j	at jth position from the x or r axis in a grid
j	jth node in FEM
$j + 1/2$	midway between j and $j + 1$
$j - 1/2$	midway between j and $j - 1$
J	at a grid's outer surface in the positive x direction
$-J$	at a grid's outer surface in the negative x direction
k	at the outer surface of the kth layer from the y axis in a grid
K	at a grid's outer surface in the positive y direction
$-K$	at a grid's outer surface in the negative y direction
m	at the mth or outermost node in a set of line elements
m	at the outer surface of the mth layer from the z axis in a grid
M	at a grid's outer surface in the positive z direction
$-M$	at a grid's outer surface in the negative z direction
n	at the surface of a 1D body, number of lamina in that body
0	at center of body

Superscripts

i	at current time or at time i
$i + 1$	at the next step after the current time step, at time $t + \Delta t$
$i - 1$	at time step just preceding current time step, at time $t - \Delta t$

References

[1] Hobbes, P.V., *Ice Physics*, Oxford University Press, London, pp. 60–78, 1974.

[2] Denbigh, K., *The Principles of Chemical Equilibrium*, 3rd edn, Cambridge University Press, London, pp. 257–261, 1971.

[3] Schwartzberg, H.G., Effective heat capacities for the freezing and thawing of foods. *J. Food Sci.*, **41(1)**, pp. 152–156, 1976.

[4] Schwartzberg, H.G., Effective heat capacities for the freezing and thawing of foods. *Freezing, Frozen Storage and Freeze-Drying*, Int. Inst. Refrig., Paris, pp. 303–310, 1977.

[5] Schwartzberg, H., *Mathematical Analysis of the Freezing and Thawing of Foods*, tutorial notes, Detroit Summer Meeting AIChE, pp. 1–39, 1981.

[6] Schwartzberg, H.G., Thermodynamics of food freezing. *Encyclopedia of Agricultural, Food and Biological Engineering*, ed. D.R. Heldman, Marcel Dekker, New York, pp. 1044–1047, 2003.

[7] Riedel, L., On the problem of bound water in meat. *Kaltetechnik*, **13**, pp. 122–28, 1961.

[8] Duckworth, R.B., Differential thermal analysis of frozen food systems, the determination of unfreezable water. *J. Food Technol.*, **6**, pp. 317–327, 1971.
[9] Pham, Q.T., Calculation of bound water in frozen food. *J. Food Sci.*, **52**, pp. 210–212, 1987.
[10] Rjutov, D.G., Influence of bound water on ice formation in foods during their freezing. *Refrig. Eng.*, **5**, pp. 32–37, 1976 (in Russian).
[11] Riedel, L., Calorimetric investigation of the freezing of fish meat. *Kaltetechnik*, **8**, pp. 374–377, 1956.
[12] Riedel, L., Calorimetric investigation of the meat freezing process. *Kaltetechnik*, **9**, pp. 38–40, 1957.
[13] Riedel, L., Calorimetric investigation of the freezing of egg white. *Kaltetechnik*, **9**, pp. 342–345, 1957.
[14] Riedel, L., Calorimetric investigation of the freezing of white bread. *Kaltetechnik*, **11**, pp. 41–43, 1959.
[15] Riedel, L., Calorimetric investigation of yeast. *Kaltetechnik-Klimatisirung*, **9**, pp. 291–293, 1968.
[16] Rektorys, K., Sequences and series with variable terms (Chapter 15). *Survey of Applicable Mathematics,* ed. K. Rektorys, MIT Press, Cambridge, pp. 684, 1969.
[17] Bartlett, L.H., *Part II – A Mathematical and Thermodynamic Determination*, *The Specific Heat of Foodstuffs*, University of Texas Engineering Research Series No. 40, University of Texas, Austin, TX, pp. 29–39, 1944.
[18] Bartlett, L.H., A thermodynamic examination of the latent heat of food. *Refrig. Eng.*, **47**, pp. 377–340, 1944.
[19] Lescano, C.E., Predicting freezing curves in codfish fillets using the ideal binary solution approximation, M.S. thesis, Michigan State University, East Lansing, MI, 1973.
[20] Heldman, D.R., Food properties during freezing. *Food Technol.*, **36(2)**, pp. 92–96, 1982.
[21] Heldman, D.R., Predicting the relationship between unfrozen water fraction and temperature during freezing using freezing point depression. *Trans. ASAE*, **17**, pp. 63–72, 1974.
[22] Miles C.K., Meat freezing – why and how? *Proceedings Meat Research Inst. Symposium No. 3*, **15**, Meat Research Inst., Bristol, pp. 1–15, 1974.
[23] Miles, C.A., The thermophysical properties of frozen foods. *Food Freezing Today and Tomorrow*, Spring-Verlag, London, pp. 45–65, 1991.
[24] Mellor, J.D., Thermophysical properties of foodstuffs. 2 Theoretical aspects. *Bulletin IIR*, **58**, pp. 569–584, 1978.
[25] Fikiin, A.G., Ice content prediction methods during food freezing: a survey of Eastern European literature. *J. Food Eng.*, **38**, pp. 331–339, 1999.
[26] Fleming, A.K.. Calorimetric properties of lamb and other meats. *J. Food Technol.*, **4**, pp. 199–215, 1969.
[27] Maltini, E., Thermal properties and structural behavior of fruit juices in the pre-freezing stage of freeze drying. *Freeze Drying and Advanced Food*

Technology, eds S.A. Goldblith, L. Rey & W.W. Rothmeyer, Academic Press, London, pp. 121–129, 1949.

[28] Jensen, K.N., Jorgensen, B.M. & Nielsen, N., Low temperature transitions in cod and tuna determined by differential scanning calorimetry. *Lebensmittel-Wissenschaft und Technologie*, **36**, pp. 369–374, 2003.

[29] Chen, C.S., Thermodynamic analysis of the freezing and thawing of foods: ice content, enthalpy and apparent specific heat. *J. Food Sci.*, **50**, pp. 1158–1162, 1985.

[30] Chen, C.S., Thermodynamic analysis of the freezing and thawing of foods: ice content and Mollier diagram, *J. Food Sci.*, **50**, pp. 1163–1167, 1985.

[31] Chen, C.S., Effective molecular weights of aqueous solutions and liquid foods calculated from freezing point depression. *J. Food Sci.*, **51**, pp. 1537–1539, 1553, 1986.

[32] Succar, J. & Hayakawa, K.I., Empirical formulae for predicting thermal physical properties of food freezing or defrosting temperatures. *Lebensmittel-Wissenschaft und Technologie*, **16**, pp. 326–331, 1983.

[33] Pham, Q.T., Prediction of calorimetric properties and freezing times of foods from composition data, *J. Food Eng.*, **30**, pp. 95–107, 1996.

[34] Cogné, C., Andrieu, J., Laurent, P., Besson, A. & Nocquet, J., Experimental data and modeling of thermal properties of ice creams. *J. Food Eng.*, **58**, pp. 331–341, 1996.

[35] Pham, Q.T., Wee, H.K., Kemp, R.M. & Lindsay, D.T., Determination of the enthalpy of foods by an adiabatic calorimeter, *J. Food Eng.*, **21**, pp. 137–156, 1994.

[36] Lindsay, D.T. & Lovatt, S.J., Further enthalpy values of foods measured by an adiabatic calorimeter, *J. Food Eng.*, **23**, pp. 95–107, 1994.

[37] Schwartzberg, H. & Liu, Y., Ice crystal growth on chilled scraped surfaces, paper 2g, AIChE Summer National Meeting, San Diego, CA, pp. 1–31, 1990.

[38] Nahid, A., Bronlund, J.E., Cleland, D.J., Oldfield, D.J. & Philpot, B., Prediction of thawing and freezing in bulk palletized butter. *9th Int. Congr. Engineering and Food*, Montpellier, France, 2004.

[39] Fennema, O.R., Powrie, W.D. & Marth, E.H., *Low Temperature Preservation of Foods and Living Matter*, Marcel Dekker, New York, pp. 186–190, 1973.

[40] Bomben, J. & King, C.J., Heat and mass transport in apple tissue. *J. Food Eng.*, **17**, pp. 615–632, 1982.

[41] Mazur, P., Cryobiology: the freezing of biological systems. *Science, NY*, **168**, pp. 939–949, 1970.

[42] Lentz, C.P., Thermal conductivities of meats, fats, gelatin gels and ice. *Food Technol.*, **15(5)**, pp. 243–247, 1961.

[43] Jason, A.C. & Long, R.A.K., The specific heat and thermal conductivity of fish muscle eutectics. *Proc. 9th Int. Congr. Refrig.*, Vol. 2, Int. Inst. Refrig., Paris, pp 160–169, 1955.

[44] Willix, J., Lovatt, S.J. & Amos, N.D., Additional thermal conductivities of foods measured by a guarded hot plate, *J. Food Eng.*, **37(2)**, pp. 159–174, 1998.
[45] Pham, Q.T. & Willix, J., Thermal conductivity of fresh lamb meat, offals and fat in the range −40°C to +30°C. *J. Food Sci.*, **54(3)**, pp. 508–515, 1989.
[46] Saad, Z. & Scott, E.P., Estimation of temperature dependent thermal properties of basic food solutions during freezing. *J. Food Eng.*, **28**, pp. 1–19, 1996.
[47] Reynaud, T., Briery, P., Andrieu, J. & Laurent, M., Thermal properties of model foods in the frozen state. *J. Food Eng.*, **15**, pp. 83–99, 1992.
[48] Plank, R., Die gefriedauer von eisblocken (Freezing times for ice blocks), *Zeitschrift fur die gesamte Kalte-Industrie*, **XX(6)**, pp. 109–114, 1913.
[49] Plank, R., Beitrage zur berechnung und bewertung der gefriergeschwindigkeit von lebensmitteln (Calculation and validation of freezing velocities in foods). *Beihefte zur Zeitschrift fur die gesamte Kalte-Industrie*, **3(10)**, pp. 1–22, 1941.
[50] Lopez-Leiva, M. & Hallstrom, B., The original Plank equation and its use in the development of food freezing rate predictions. *J. Food Eng.*, **58**, pp. 267–275, 2003.
[51] Rjutov, D.G., Die Anwendung kunstlicher kalte in der UdSSR. *Berichte fur den 7*Int. Kalte-Kong., Moskau and Leningrad, Verlag der Nahrungsmittelindustrie, **S**, pp. 60, 1936.
[52] Carslaw, H.R. & Jaeger, J.C., *Conduction of Heat in Solids*, 2nd edn, Oxford University Press, London, 1959.
[53] Ede, A.J., The calculation of the rate of freezing and thawing of foodstuffs, *Modern Refrigeration*, **17**, pp. 52–55, 1949.
[54] Nagoaka, J., Takaji, S. & Hohani, S., Experiments on fish freezing in blast freezers. *Proc. 9th Int. Congr. Refrig.*, Int. Inst. Refrig., Paris, paper 4, pp. 105–110, 1955.
[55] Cleland, A.C. & Earle, R.L., Freezing time prediction for foods – a simplified procedure. *Int. J. Refrig.*, **5**, pp. 98–106, 1982.
[56] Hung, Y.C. & Thompson, D.R., Freezing time prediction for slab shape foodstuffs by an improved analytical method. *J. Food Sci.*, **48(2)**, pp. 555–560, 1983.
[57] Levy, F.L., Calculating the freezing time of fishes. *J. Refrig.*, **1**, pp. 55–58, 1958.
[58] Salvadori, V.O., de Michelis, A. & Mascheroni, R.H., Prediction of freezing times for regular multi-dimensional foods using simple formulas. *Lebensmittel-Wissenschaft und Technologie*, **30**, pp. 30–35, 1997.
[59] Cleland, D.J., Cleland, A.C. & Earle, R.L., Prediction of freezing and thawing times for multidimensional shapes by simple methods, Part I – regular shapes. *Int. J. Refrig.*, **10**, pp. 156–164, 1987.
[60] Pham, Q.T., Extension of Plank's equation for predicting freezing times of foodstuffs of simple shape. *Int. J. Refrig.*, **7**, pp. 377–383, 1984.

[61] Harris, M.B., Carson, J.L., Willix, J. & Lovatt, S.J., Local heat-transfer coefficients in a model lamb carcass. *J. Food Eng.*, **61(3)**, pp. 421–429, 2004.
[62] Özişik, N., *Heat Conduction*, Wiley-Interscience, New York, 1980.
[63] Mannaperuma, J.D. & Singh, R.P., Prediction of freezing and thawing times of foods using a numerical method based on enthalpy formulation. *J. Food Sci.*, **53(2)**, pp. 626–630, 1988.
[64] Crank, J. & Nicholson, P., A practical method for the numerical integration of solutions of partial differential equations of heat conduction type. *Proc. Cambridge Philosophical Society*, **43**, pp. 50–67, 1947.
[65] Cleland, A.C., *Food Refrigeration Processes*, Elsevier Applied Science, London, pp. 42–92, 99–152, 1990.
[66] Press, W.H., Flannery, B.P., Teukolsky, S.A. & Vetterrling W.T., *Numerical Recipes*, Cambridge University Press, Cambridge, pp. 41–42, 1987.
[67] Lees, M., A linear three level difference scheme for quasi-parabolic equations. *Maths. Comput.*, **20**, pp. 516–522, 1966.
[68] Eyres, N.R., Hartree, D.R., Ingham, J., Jackson, R., Sarjant, R.J. & Wagstaff, J.B., The calculation of variable heat flow in solids. *Trans. Royal Society, London*, **A240**, pp. 1–58, 1946.
[69] Mannaperuma, J.D. & Singh, R.P., A computer-aided method for the prediction of properties and freezing/thawing times of foods. *J. Food Eng.*, **9(4),** pp. 275–304, 1989.
[70] Toumi, S., Amarante, A. Lanoiselle, J.L. & Clausse, D., Freezing of food-stuffs: experimental determination of calorimetric properties and freezing simulation using an enthalpy-temperature formulation. *9th Int. Congr. Engineering and Food*, Montpellier, France, 2004.
[71] Pham, Q.T., A fast, unconditionally stable finite difference scheme for heat conduction with phase change. *Int. J. Heat Mass Transf.*, **28(11)**, pp. 2079–2084, 1985.
[72] Peaceman, D.W. & Ratchford, H.H., The numerical solution of parabolic and elliptic differential equations. *J. SIAM*, **3(1)**, pp. 28–41, 1955.
[73] Fleming, A.K., The numerical calculation of freezing processes. *Proc. 13th Int. Congr. Refrig.*, **2**, Int. Inst. Refrig., Paris, pp. 303–311, 1971.
[74] Fleming, A.K., Application of a computer program to freezing processes. *Proc. 13th Int. Congr. Refrig.*, **2**, Int. Inst. Refrig., Paris, pp. 403–410, 1971.
[75] Brisson Lopez, J.M. & Domingos, J.J.D., The numerical computation of freezing processes in bodies of arbitrary shape. *Proc.* 15^{th} *Int. Congr. Refrig.*, **2**, Int. Inst. Refrig., Paris, pp. 605–616, 1979.
[76] Barth, F.M., The treatment of unsteady state heat conduction with change of phase. *Refrigeration Science and Technology*, **2**, pp. 225–230, 1984.
[77] Brisson Lopez, J.M., Application of the EXPIMP system to phase change problems in orthogonal and curvilinear coordinates. *Proc. 16th Int. Congr. Refrig.*, **2**, Int. Inst. Refrig., Paris, pp. 603–610, 1983.
[78] Kunis, J., Barth, F.M. & Nowotny, S., A new interactive method of finite differences for calculation of freezing processes. *Proc. 16th Int. Congr. Refrig.*, **2**, Int. Inst. Refrig., Paris, pp. 611–616, 1983.

[79] Califano, A.N. & Zartitzky, N.E., Simulation of freezing and thawing heat conduction in irregular two-dimensional domains by a boundary-fitted grid method. *Lebensmittel-Wissenschaft und Technologie*, **30**, pp. 70–76, 1997.
[80] Comini, G., Del Giudice, S., Lewis, R.W. & Zienkiewicz, O.C., Finite element solution of non-linear heat conduction problems with special reference to phase change. *Int. J. Num. Meth. Eng.*, **8**, pp. 613–624, 1974.
[81] Purwadaria, H.K. & Heldman, D.R., A finite element method for predicting of freezing rates in foods with anomalous shapes. *Trans. ASAE*, **25**, pp. 827–832, 1982.
[82] Hayakawa, K., Nonino, C., Succar, J., Comini, G. & Del Giudice, S., Two dimensional heat conduction in foods undergoing freezing, development of computerized model. *J. Food Sci.*, **48**, pp. 1849–1953, 1983.
[83] Cleland, D.J., Cleland, A.C., Earle, R.L. & Byrne, S.J., Prediction of rates of freezing, thawing and cooling in solids of arbitrary shape using the finite element method. *Int. J. Refrig.*, **7**, pp. 6–13, 1985.
[84] Abdalla, H. & Singh, R.P., Simulation of freezing and thawing in foods using a finite element method. *J. Food Proc. Eng.*, **7**, pp. 273–286, 1985.
[85] De Cindio, B., Iorio, G. & Romano, G., Thermal analysis of freezing of ice cream brickettes by the finite element method. *J. Food Sci.*, **50**, pp. 1463–1467, 1985.
[86] Rebellato, L, Del Giudice, S. & Comini, G., Finite element analysis of freezing processes in foodstuffs. *J. Food Sci.*, **43**, pp. 239–243, 250, 1985.
[87] Wang, D.Q. & Kolbe, E., Analysis of food brick freezing using a PC based finite element package. *J. Food Eng.,* **21**, pp. 521–530, 1994.
[88] Huan, Z., Hu, S. & Ma, Y., Numerical simulation and analysis for quick-frozen food processing. *J. Food Eng.,* **60**, pp. 267–273, 2003.
[89] Cogné, C., Laurent, P. & Andrieu, J., Heat transfer model of commercial ice cream freezing. *9th Int. Congr. Engineering and Food*, Montpellier, France, 2004.
[90] Tremeac, B. Lefeuve, J. Hayert, M., Le Bail, A. & Moes, N., Thermo-mechanical modeling during freezing. *9th Int. Congr. Engineering and Food*, Montpellier, France, 2004.
[91] Scheerlinck, N, Verboven, P., Fikiin, K.A., De Baerdemaeker, J. & Nicolai, B.M., Finite element computation of unsteady state phase change heat transfer during freezing and thawing of food using a combined enthalpy and Kirchoff transform method. *Trans. ASAE*, **44(2)**, pp. 429–438, 2001.
[92] Purwadaria, H.K., *A Numerical Prediction Model for Food Freezing Using Finite Element Methods*, PhD thesis, Michigan State University, East Lansing, MI, 1980.
[93] Huebner, K.H., Thornton, E.A. & Byrom, T.G., *The Finite Element for Engineers*, 3rd edn, John Wiley, New York, 1995.
[94] Zienkiewicz, O.C. & Taylor, R.C., *The Finite Element, The Basis*, 5th edn, Vol. 1, Butterworth and Heineman. Oxford, 2000.
[95] Segerlind, L.J., *Applied Finite Element Analysis*, 2nd edn, John Wiley, New York, 1984.

[96] Lewis, R.W., Morgan, K., Thomas, H.R. & Seetharamu, K.N., *The Finite Element Method in Heat Transfer Analysis*, John Wiley, New York, 1996.
[97] Huang, H.C. & Usmani, A.S., *Finite Element Analysis of Heat Transfer*, Springer-Verlag, Berlin, 1994.
[98] Meyers, G.E., Finite elements (Chapter 9). *Analytical Methods of Conduction Heat Transfer*, McGraw-Hill, New York, pp. 320–428, 1971.
[99] Pham, Q.T., The use of lumped capacitance in the finite element solution of heat conduction problems with phase change. *Int. J. Heat Mass Transf.*, **29(2)**, pp. 285–291, 1986.
[100] Carroll, N., Mohtar, R. & Segerlind. L.J., Predicting the cooling time of irregular shaped food products, *J. Food Proc. Eng.*, **19**, pp. 385–401, 1996.
[101] Zienkiewicz, O.C. & Parekh, C.J., Transient field problems: two-dimensional and three-dimensional analysis by isoparametric finite elements. *Int. J. Num. Meth. Eng.*, **2**, pp. 61–71, 1970.
[102] Cheung, Y.K., Lo, S.H. & Leung, A.Y.T., *Finite Element Implementation*, Blackwell Science, 1996.
[103] Maggioli, C., Balsa-Canto, E. & Chiumenti, M., FEM based advanced tools for simulation of food preservation processes. *9th Int. Congr. Engineering and Food*, Montpellier, France, 2004.
[104] MacNeal, B.E., FEA: A guide to the future (Chapter 9). *What Every Engineer Should Know About Finite Element Analysis*, 2nd edn, ed. J.C. Brauer, Marcel Dekker, New York, pp. 289–313, 1993
[105] ABAQUS/Standard, www.hks.com/products-standard
[106] Heald, E.E., Johnson, D.H. & Roth D.E., *ANSYS: Heat Transfer Users Guide for Revisions 5.1*, ANSYS Inc., Houston, 1985.
[107] COMSOL AB, *FEMLAB Users Guide*, COMSOL Inc., Burlington, MA, 2004.
[108] ALGOR, www.algor.com/products/analysis-types/thermal/trans.therm/asp
[109] Shapiro, A.D., *Topaz 3-D Finite Element Heat Transfer*, Energy Science and Technology Center, U.S.D.O.E, Oakridge, TN, 2002.
[110] ABAQUS Inc., *ABAQUS Expands Educational Program with ABAQUS Student Edition*, www.hks.com
[111] MATLAB, *MATLAB High Performance Numerical Computation and Visualization Software, Users Guide*, Math Works, Natick, MA, 1993.
[112] Department of Mechanics and Materials, University of Lund, *CALFEM, a Finite Element Toolbox to MATLAB, Version 3.3*, Structural Mechanics LTH, Sweden, 1999.